NTNU – Trondheim
Norwegian University of
Science and Technology

Terbium Doped ITO Thin Films Prepared by an Aqueous Sol-Gel Method

Sandra Helen Skjærvø

Chemical Engineering and Biotechnology
Submission date: June 2013
Supervisor: Tor Grande, IMTE
Co-supervisor: Mari-Ann Einarsrud, IMT
Tor Olav Løveng Sunde, IMT

Norwegian University of Science and Technology
Department of Materials Science and Engineering

Assignment

In this work we wish to prepare thin films of indium tin oxide (ITO) doped with the rare earth element terbium by an aqueous sol-gel method and the deposition method spin-coating. The method is very attractive in regards to environmentally friendly precursors (no organic solvents) and its low cost. Rare earth elements exhibit the unique property of converting the frequency of electromagnetic radiation. The aim is to investigate whether the rare earth can be implemented homogeneously into the ITO crystal structure and if the prepared thin films retain the good optical and electrical properties of the host when doped. The thin films are characterised in regards to microstructure, crystal structure, electrical properties and optical properties.

Abstract

Transparent conducting oxides (TCOs) combine the properties of optical transparency in the visible region of the electromagnetic spectrum and a near-metallic electrical conductivity. This combination make them very applicable in many technological areas. The prime candidate amongst the TCOs is indium oxide doped with tin oxide, usually referred to as indium tin oxide (ITO). The aim of this work was to dope this incredible material with the rare earth element terbium and investigate the effects of the dopant on the properties of the host. If successful, one could possibly enhance the optical properties by introducing luminescence.

An environmentally friendly aqueous sol–gel process was used to fabricate nanocrystalline thin films and powders of indium tin oxide doped with terbium. A stable solution was prepared from indium nitrate precursor, tin acetate and terbium nitrate together with acetic acid and ethylene glycol. The ITO:Tb thin films consisted of spherical nanocrystalline particles and were of high homogeneity and phase purity. Grain size and crystallite size of the thin films seemed to be independent on terbium concentration. The powders were also nanocrystalline but showed some impurities at high terbium concentrations. The deposited thin films exhibited very good and reproducible electrical conductivity and optical transparency. The specific resistance of the thin films declined with the terbium concentration, but not to an extent that it was detrimental to the electrical properties. The specific resistance increased from $5.1 \cdot 10^{-3} \Omega cm$ for a doping concentration of 0.5 cation% terbium to $5.2 \cdot 10^{-2} \Omega cm$ for a doping concentration of 10 cation% terbium. Post-annealing of the prepared thin films in air up to $300°C$ showed a decrease in the conductivity, which became more prominent with the terbium concentration in the thin films. This decrease was attributed to oxidation of terbium and tin and thereby reduction of charge carrier concentration. The de-

crease in conductivity as a result of the doping by itself seemed to be equally important as the reduction caused by oxidation. The optical transmission seemed independent on terbium concentration and had a maximum of 92 % in the visible spectrum and a band absorption edge around 350 nm. A decrease in the lattice parameter of the thin films was observed for the lowest terbium concentrations followed by an increase with the terbium concentration. The latter effect was attributed to the larger size of Tb^{3+} compared to In^{3+}. The lattice parameter of the thin films also increased with the number of deposited layers, probably due to strain between the substrate and the thin film.

Absorption and emission properties of the materials were not studied, and therefore no conclusions could be made about the luminescent properties of the ITO:Tb materials.

Sammendrag

Transparente ledende oksider (TCOer) kombinerer egenskapene optisk gjennomsiktighet i det synlige spekteret av elektromagnetisk stråling og en nær-metallisk elektrisk ledningsevne. Denne kombinasjonen gjør dem svær anvendelige innen mange teknologiske områder. Den fremste kandidaten blant TCO-ene er indiumoksid dopet med tinn, ofte referert til som indiumtinnoksid (ITO). Målet med dette arbeidet var å dope dette fantastiske materialet med det sjeldne jordartsmetallet terbium og undersøke effekten av dopanten på de gode egenskapene til verten. Hvis dette lykkes, kan det åpne muligheten for å forbedre de optiske egenskapene ved å introdusere luminescens.

En miljøvennlig vandig sol-gel-metode ble brukt til å fremstille nanokrystallinske tynnfilmer og pulvere av indiumtinnoksid dopet med terbium. En stabil løsning ble fremstilt av indiumnitrat-forløper, tinnacetat og terbiumnitrat sammen med eddiksyre og etylenglykol. ITO:Tb-tynnfilmene bestod av sfæriske nanokrystallinske korn og hadde høy homogenitet og faserenhet. Kornstørrelsen og krystallittstørrelsen til tynnfilmene så ikke ut til å avhenge av terbiumkonsentrasjonen. Pulverene var også nanokrystallinske, men inneholdt noen urenheter ved høye terbiumkonsentrasjoner. Tynnfilmene viste reproduserbart gode elektriske ledningsevne og optisk gjennomsiktighet. Den spesifikke ledningsevnen til tynnfilmene avtok med terbiumkonsentrasjonen, men ikke nok til å forringe de elektriske egenskapene. Den spesifikke ledningsevnen økte fra $5.1 \cdot 10^{-3} \Omega cm$ for doping konsentrasjon på 0.5 cation% terbium til $5.2 \cdot 10^{-2} \Omega cm$ for doping konsentrasjon på 10 cation% terbium. Varmebehandling av de ferdige tynnfilmene i luft opp til $300°C$ viste en reduksjon i ledningsevne, som ble mer fremtredende ved høye terbium konsentrasjoner. Denne nedgangen ble tilskrevet oksidasjon av tinn og terbium og dermed en reduksjon i ladningsbærerkonsentrasjon. Reduksjonen i ledningsevne som følge

av selve dopingen så ut til å være like viktig som reduksjon som følge av oksidasjon av tynnfilmene. Den optiske gjennomsiktigheten så ikke ut til å avhenge av terbiumkonsentrasjon og hadde en maksimalverdi på 92 % i det synlige spekteret og en båndabsorpsjonskant rundt 350 nm. En reduksjon i gitterparameter for tynnfilmene ble observert for de laveste terbiumkonsnetrasjonene, fulgt av en økning som funksjon av terbiumkonsentrasjon. Det sistnevnte ble tilskrevet den større ioneradien til Tb^{3+} i forhold til In^{3+}. Gitterparameteren til tynnfilmene økte også med antall avsatte lag, trolig på grunn av spenning mellom substratet og tynnfilmen.

Absorpsjons- og emisjonsegenskapene til materialene ble ikke undersøkt, og derfor kunne ingenting sies om de luminescerende egenskapene til ITO:Tb-materialene.

Acknowledgements

Many people have been of great importance during my work, helping me achieve what I set out to do. First, I would like to thank my supervisor, professor Tor Grande, who always filled my head with thousands of ideas after our meetings and made me believe that I could do it. I could not have asked for a better supervisor.

I would also like to thank Tor Olav Løveng Sunde for being my number one go-to-guy. Even though you were in the final part of your PhD, you always had the time to answer my questions and were a great academic discussion partner.

I am also greatful for all the academic feedback from the Solar reseach group at Department of Materials Technology including my co-supervisor professor Mari-Ann Einarsrud. They challenged me and guided me towards a greater understanding of my project. I look foreward to working with all of you again.

Several people have made it possible to conduct the laboratory work, including Astrid Salvesen and Sebastian Bete who carefully cut my thin film samples, Lars Martin Sandvik Aas who helped me with the ellipsometry measurements and Vegar Øygarden and Ørjan Lohne Fossmark for always stepping up when I had problems in the laboratory. I wish to thank all of you.

I also wish to thank my family for all the support, and foremost, my twin sister, Susanne Linn Skjærvø. You have always been the one who understands me the best. You know how to push me when I need to get moving and relaxe me when I need it the most.

Finally, I would like to thank Tormod Østmoe for being my knight in shining armour. You always know how to put a smile on my face, even in tough times.

Preface

This dissertation is the result of my work carried out the in 10th semester of my studies for obtaining Master's Degree in Chemical Engineering and Biotechnology, specialising in Materials Chemistry and Energy Technology at the Department of Materials Technology (IMT) at the Norwegian University of Science and Technology (NTNU).

The effects on the functional properties of indium tin oxide (ITO) thin films when doped with the rare earth metal ion terbium has been studied, as a continuation of the preliminary master thesis conducted during the 9th semester. Three of the samples prepared during these preliminary studies, the 0, 1 and 2 cation% terbium thin films and powders, have been used in the present work.

All of the experiments have been conducted by the author exept from the transmission spectrophotometry in Figure 5.8, which were measured at the Department of Physics at NTNU.

Contents

1 Background

Transparent conducting oxides (TCOs) demonstrate the remarkable combination of near-metallic conductivity, high transmittance of visible light and high reflectivity of infrared light [1]. As early as 1907, the first transparent conducting CdO thin film was prepared by thermal oxidation of sputtered cadmium by Badeker [2]. The interest for these materials has grown ever since. The typically wide bandgap in the TCOs give them quite unique properties, and TCOs are therefore utilised in numerous technological applications, such as flat panel displays, energy efficient windows, light emitting diods, gas sensors, photovoltaic devices, etc. [1, 3, 4, 5, 6, 7, 8]. With the aim of increasing the efficiency of solar cells, TCOs can also be utilised as host materials for luminescent species. Although they are oxides, recent research has shown that the TCOs can serve as good hosts for luminescent materials [9].

Several oxides can, by themselves or in combination with others, make a good TCO, such as In_2O_3, ZnO, SnO_2 *and* CdO [1, 10]. The prime candidate amongst the TCOs is indium oxide doped with tin oxide, usually referred to as indium tin oxide or ITO, with more than a 90% share of the market [10]. ITO has been utilised in solar cells for the last decade, as transparent electrodes [3].

Because of the formidable energy created by the sun, harvesting of sunlight by the use photovoltaic devices, or solar cells, could contribute to cover the continuous increase in the worlds energy demands. The transmission of sub-bandgap light is one of the major loss mechanisms in conventional solar cells [11], and the losses leave the efficiency of a standard solar cell as low as 15-20 % [12]. Of the many approaches to enhance the efficiency, tandem cells provide the best known example, where the efficiency can be increased

merely by adding more cells of different bandgaps to a stack [12]. Other approaches have aimed to reduce these losses by luminescence mechanisms such as upconversion, downconversion and downshifting [13]. Combining the best efficiency increasing mechanism and striving to do so with low cost materials and production methods may result in the next generation high efficiency solar cells.

With the continuous development of thin film technology and its applications, the traditional ITO thin films are unable to meet higher performance requirements. The photoelectrical properties of the ITO thin films can be improved by doping other elements [14]. Generally, rare earth ions like Eu^{3+}, Er^{3+}, Tb^{3+}, Nd^{3+}, and so forth incorporated in semiconductors may introduce luminescence by energy transfer processes. Rare earth ions trapped in host lattices have received much attention for their optical properties in terms of fundamental and technological importance [15, 16]. These host matrices effectively reduce the quenching of rare earth surface emission by shielding the rare earth ions present on the surface of the nanoparticles from the external ligands [16]. However, very few reports on synthesis and optical studies of rare earth doped In_2O_3 films have been published. If succeded, ITO thin films with luminescent properties can be utilised in a photovoltaic and thereby enhance its efficiency [12, 13, 17, 18, 19]. Luminescence in materials is not only interesting in the field of solar cells, but also in telecommunication, displays, laser materials, data storage, radiation detection, and medical applications the luminescent rare earths are playing an increasingly important role [20].

Terbium can emit light in the green part of the solar spectrum if implemented in an appropriate host. Terbium activated phosphors are today utilised in a variety of applications such as emissive displays, fluorescent lamps, LEDs and X-ray intensifying screens for medical purposes [21]. To

the authors knowledge, terbium has not previously been doped into ITO for the purpose of introducing luminescent properties to a material which is already extensively utilised for its remarkable properties in many applications today. In case of success, this novel property of ITO may create yet more applications for this remarkable TCO. But doping a TCO with impurities may affect the functional properties of the host itself, and it is therefore nescessary to investigate these effects.

Several techniques have been developed for deposition of ITO thin films, such as radio frequency sputtering [22], pulsed laser deposition [23], spray pyrolysis [24], chemical vapor deposition [3, 25], vacuum evaporation [6] and sol-gel methods [4, 10]. Sputtering is the most widely used industrial process for fabricating these thin films, but wet chemical methods, such as sol-gel, have potentially many advantages compared to physical methods. The wet chemical methods are relatively simple techniques where the composition and homogeneity down to the molecular level can readily be controlled by adjusting the process parameters, such as stability of the solution, wettability and viscosity [26]. They can also be utilised to coat larger substrates and substrates with different geometries by spin or dip coating deposition techniques [27, 28, 29]. Aqueous sol-gel methods are enviromentally friendly, inexpensive and easy [10]. It is also an advantage to be able to perform the deposition at low temperatures to avoid diffusion of alkali ions from the glass substrates into the thin film and to avoid coarsering of the nanocrystalline particles [3]. Nano-sized powders will often give advantages when producing ceramic materials. The small particle size will make the powders easier to pack into dense objects to provide increased strength and hardness [26]. Increased specific heat capacity, improved thermal expansion properties, lower thermal conductivity and improved magnetic properties are also results due to their nano-size [30].

2 Objective

The widespread research carried out on TCOs and ITO the last decades, has resulted in numerous applications for these materials. In recent years, the Inorganic Materials and Ceramics Research Group at the Department of Material Science at NTNU has contributed to the development of ITO thin films and has achieved to improve the sol-gel techniques [10, 31]. The work for this master thesis aimed to reveal if terbium at both low and high concentrations could be implemented into the host matrix of indium tin oxide without reducing the host material's transparency and electrical conductivity. The longterm goal for subsequent work would be to find out if terbium, alone or in combination with other impurity species, can contribute in developing the next generation solar cells by introducing the property of anti-Stokes upconversion [11, 12, 17, 19]. Terbium was chosen because of its intermediary position amongst the rare earths and because of its ability to change oxidation number easily.

Preparation of thin films of ITO doped with 0.5, 1, 2, 5 and 10 cation% Tb was performed by spin coating. The method used was a modified Pechini sol-gel method with the cheap and environmentally friendly precursors acetic acid and ethylene glycol. The thin films were analysed with respect to optical transmission, electrical conductivity, composition, crystal structure and microstructure. Bulk samples of nanocrystalline powders were also synthesised from the ITO solutions. These powders were analysed with respect to composition and chemical composition to verify that the solutions had been prepared correctly.

3 Literature survey

3.1 Indium oxide and ITO

3.1.1 Crystal structure

Pure indium oxide (In_2O_3) crystallises with the bixbyite structure at ambient conditions. Figure 3.1a shows the crystal structure of In_2O_3. This body-centered C-type rare earth sesquioxide lattice structure is similar to fluorite and belongs to the space group Ia3, number 206 [5]. Unlike fluorite, one fourths of the anions are missing, and this results in a rather complex structure with empty oxygen lattice sites. The unit cell consists of 80 atoms with 32 cations divided into two positions. As shown in Figure 3.1b, each cation resides at the center of a distorted cube, with six corners occupied by oxygens. All 8b cations are coordinated to six oxygens at a distance of 2.18 Å and to two empty oxygen lattice positions, which lie along a body diagonal of the cube. The 24d cations exhibit less symmetry, as they are

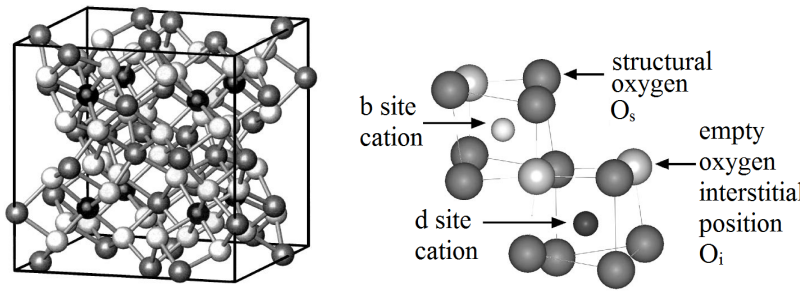

Figure 3.1: *(a) Crystal structure of In_2O_3. Black, shaded and white spheres represent resprectively 8b indium, 24d indium and 48e oxygen atoms in a convetional unit cell* [32]. *(b) Cation positions in pure In_2O_3 [5].*

coordinated to six oxygens at three distances (2.13, 2.19, and 2.23 Å) and to two empty oxygen lattice positions along a face diagonal of the cube. These empty oxygen lattice positions, also called the 16c positions, are in most literature referred to as interstitial positions [5, 6, 7, 8, 32]. The 48 oxygen anions are coordinated to four cations and occupy the general position 48e. Indium oxide is non-stoichiometric with respect to oxygen, leading to the formula $In_2O_{3-\delta}$. Delta (δ) depends on impurity concentration and synthesis conditions, such as oxidizing or reducing atmosphere, but can be as high as 0.01 [33]. A diffractogram by Sunde *et al.* [10], given in Figure 3.2, show the characteristic bixbyite structure of indium oxide.

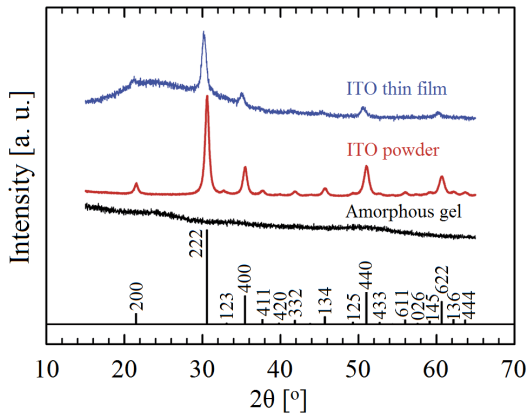

Figure 3.2: *XRD patterns of an amorphous ITO gel after evaporation of the solvent, ITO powder after calcination at 400 °C and an ITO thin film of 10 deposited layers [10]. The gel and the powder contain 5 cation% Sn, while the film contains 10 cation% Sn. The pattern for the cubic In_2O_3 with the space group Ia3 is given at the bottom.*

Tin doped indium oxide, with tin content up to about 20 cation% Sn ($In_{2-x}Sn_xO_3$,x<0.2) [4], can also crystallise with the bixbyite structure [33, 34, 35]. The phase diagram of ITO is shown in Figure 3.3a. The In-

rich side of the phasediagram is shown in Figure 3.3b. The diagrams show that tin will not be dissolved in the indium oxide structure if it is in an equilibrium state. This means that ITO thin films with 10 cation% tin are thermodynamically metastable at ambient conditions. Preparation of nanocrystalline ITO is usually conducted at as low temperature as possible to form a crystallisation in order to prevent particle coarsening. Since long-range diffusion is kinetically limited during crystallisation, metastable phases often crystallise depending on the precursors [35]. Rhombohedral ITO can form at low temperatures and high tin levels, but can be transformed back to the cubic phase when heated to around 900 $°C$ [35].

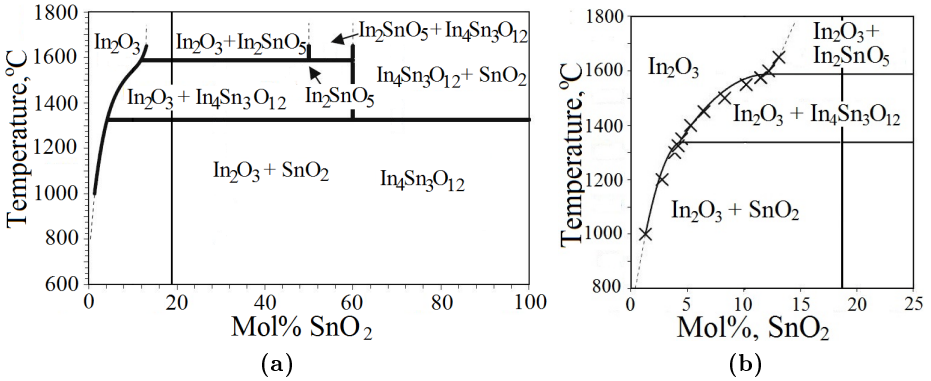

Figure 3.3: *(a) Phase equilibria in the $In_2O_3 - SnO_2$-system [34]. The composition of 10 cation% Sn (18.18 mol%) is marked as a vertical line.* (b) *The In_2O_3 rich side of the $In_2O_3 - SnO_2$ of the phase diagram, showing the solid solubility range of SnO_2 in In_2O_3 [34]. The composition of 10 cation% Sn (18.18 mol%) is marked as a vertical line.*

When substituted into the lattice structure of indium oxide, the Sn^{4+}cations have a preference for the more symmetrical 8b positions, shown by Gonzàlez *et al.* [5] in 2004. But since there are 24 d-sites and only 8 b-sites in each

unit cell, the tin occupancy will be considerable in both sites. If one only consider the radii of six-coordinated In^{3+} and Sn^{4+}, of 0.80 Å and 0.69 Å [36], respectively, one would expect a lattice contraction when substituting In^{3+} for Sn^{4+}. Interestingly, this is not so straight forward. Frank and Köstlin [37] showed how the lattice parameter changes in oxidizing and reducing conditions when doping indium oxide thin films with tin [37], given in Figure 3.4a. At low doping concentrations ($c_{Sn}<$ 2 atom%) one can see a small decrease in lattice parameter consistent with the smaller radius of Sn^{4+}. This is followed by a remarkable increase in the lattice parameter with the tin concentration. The increase at higher doping levels can be attributed to the higher effective charge of the Sn^{4+}-ions, which causes a repulsion force which cannot be completely compensated by the shielding electrons [38]. ITO and In_2O_3 are usually prepared in reducing conditions to constrain the amount of compensating interstitial oxygens in the structure and thereby maximise the oxygen vacancies. The lattice parameter of ITO when produced in reducing conditions is usually in the range 10.118 - 10.31 Å [3], which is larger than that of pure In_2O_3 with a lattice parameter of 10.117 Å [5, 6, 7, 8, 10, 32]. When prepared at oxidizing conditions, extra oxygen atoms occupy the remaining interstitial 16c positions in each cube to compensate the extra positive charge by the Sn^{4+} ions [6]. At ambient conditions and normal oxygen partial pressures, the oxygen vacancy concentration is negligible [5, 6], and the tin doped indium oxide can therefore be described by the molecular formula $In_{2-x}Sn_x^{\bullet}(O_i)''_{x/2}O_3$ [5, 8].

Figure 3.4a also shows that the lattice parameters in the reduced state are always larger than in the oxidized state. The difference between the oxidized and reduced states at a given tin concentration is shown in Figure 3.4b together with the measured difference of the carrier concentrations in both states. It is clear that both differences are proportional. They increase

linearly with the doping concentration up to a limit which is identical to the solubility of tin in In_2O_3 of c_{Sn}, = 5-6 atom% , and then they remain constant.

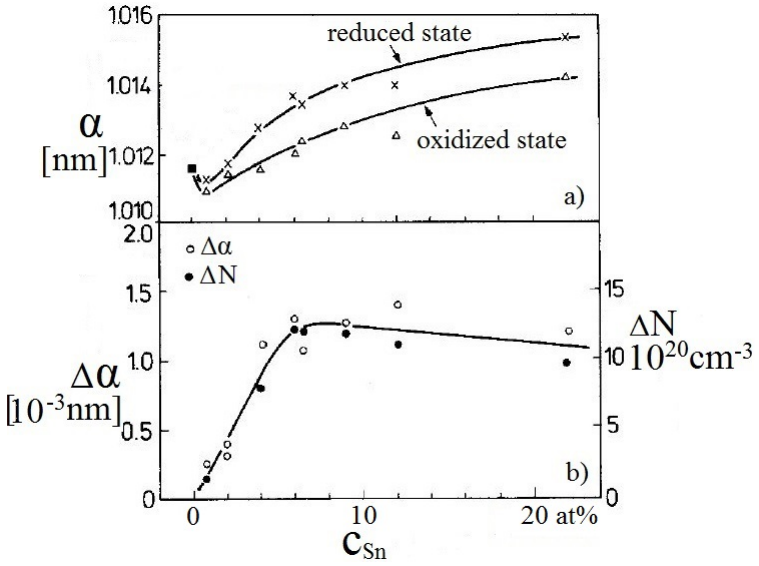

Figure 3.4: *(a) Lattice constants of $In_2O_3 : Sn$ layers, annealed under oxidizing (Δ) and reducing (x) conditions, vs. tin doping concentration. Calculation from (800) x-ray reflex. (b) Correlation of lattice constant decrease ($\circ$) with carrier concentration decrease ($\bullet$) during oxidation of reduced layers [37].*

The thickness of the thin films also seems to affect the lattice parameter of the ITO. A decrease in the lattice parameter as a function of number of deposited layers has been reported by Kim *et al.* [39], where layers of ITO thin films of thicknesses in the range of 30-700 nm were prepared by pulsed laser deposition at $300°C$ and a reducing environment of 10 mTorr oxygen. This is illustrated in Figure 3.5. The explanation for for this decrease is

probably due to the difference in expansion coefficient between the glass substrate ($4.6 \cdot 10^{-6}/°C$ [39]) and the thin film ($7.2 \cdot 10^{-6}/°C$ [39]), causing a negative thermal strain between the more expanding thin film and the less expanding substrate which decreases as the thin film gets thicker.

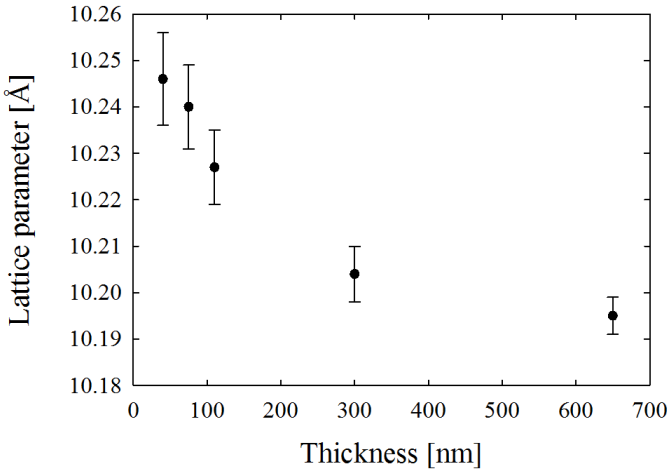

Figure 3.5: *Lattice parameter of ITO as a function of thickness of the thin film. Modified from Kim et al. [39].*

3.1.2 Nanostructure, microstructure and homogeneity

Sunde *et al.* [10] showed that the film thickness of ITO thin films increases linearily with the number of deposition, with each deposition adding around 17 ± 1 nm to the total thickness. These thin films were prepared by an aqueous sol-gel method utilising acetic acid and ethylen glycol, a concentration of 0.2 M and 3 weight% PVA. The same work reported spherical morphology of the grains in the film which had an average size of 16 ± 3 nm. This suggested that the grain size reflected the thickness of each deposited

layer and that each deposited layer was similar to a monolayer of particles, even after the final annealing step.

Also the homogeneity of a thin film consisting of several layers has shown to increase as the number of layers increases. Guo *et al.* [40] presented atomic force microscopy (AFM) images of the surfaces of epitaxially grown ITO thin films of varying numbers of monolayers (ML), given in Figure 3.6. The roughness appeared to reach a minimum at about 200 ML, where the thin film became atomically smooth [40].

Sunde *et al.* [10] found that the crystallite sizes of ITO seemed to be unaffected by the tin content, but increased as a result of higher calcination temperature.

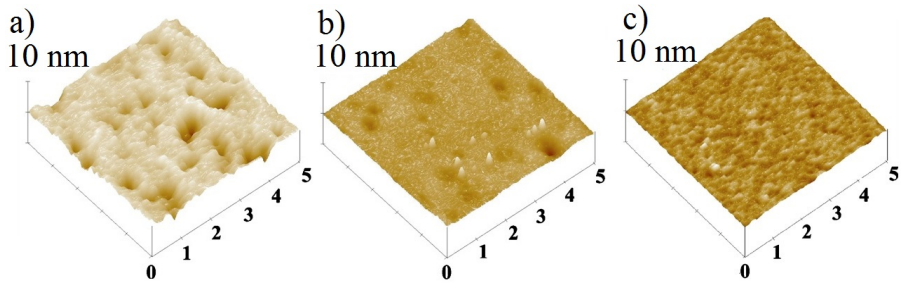

Figure 3.6: *AFM 3D images 5 x 5 μm^2: a) 5 ML, b) 20 ML, and c 200 ML ITO thin-films grown on $LaAlO_3$ substrates [40].*

3.1.3 Defect structure and electrical conductivity

Given the importance of indium oxide and ITO, surprisingly little is known with certainty about its defect chemistry. Undoped In_2O_3 is an intrinsic n-type semiconductor [41]. This semiconductivity depends on the conditions of preparation, grain boundaries and impurities, which can give a poor reproducibility of experimental data [41]. The free electrons are

donated from oxygen vacancies, according to Equation 1 and 2, concluded by De Wit *et al.* in the 1970s [41, 42, 43].

$$O_O^x \rightarrow \frac{1}{2}O_2(g) + V_O^{\bullet\bullet} + 2e^{'} \tag{1}$$

$$K_{red} = pO_2^{1/2}\left[V_O^{\bullet\bullet}\right] n^2 \tag{2}$$

When indium oxide is prepared at high oxygen pressures, oxygen goes into the interstitial position, as the electroneutrality in Equation 3 shows. Many measurements have concluded that the oxygen interstitials are a minority species compared to the oxygen vacancies and that indium oxide is a oxygen deficient n-type conductor [5, 8, 37, 41, 42, 43]. But even at the maximal oxygen vacancy population of about 1 anion% at reducing conditions, the free electron concentration is limited.

$$n + 2\left[O_i^{''}\right] = p + 2\left[V_O^{\bullet\bullet}\right] \tag{3}$$

Doping with tin can be described by simple Kröger-Vink notation, given in Equations 4. Here we assume only Sn^{4+} cations, as Sn^{2+}only occur at strongly reducing conditions, shown by Köstlin's Mössbauer spectroscopy measurements in 1975 [44]. ITO is an n-type degenerate semiconductor with an optical bandgap of about 3.75 eV. If prepared under reducing conditions, the interstitial oxygens will desorb, and as a result, each tin donates one electron to the conduction band, as seen from Equation 5.

$$2SnO_2 \xrightarrow{In_2O_3} 2Sn_{In}^{\bullet} + O_i^{''} + 3O_o^x \tag{4}$$

$$O_i'' \rightarrow \frac{1}{2}O_2 + 2e' \tag{5}$$

At high tin concentrations or high oxygen pressures neutral Sn-oxygen interstial associates, $\left[2Sn_{In}^{\bullet}O_i''\right]^x$, form where each interstitial oxygen is loosely bound to two tin ions. When the oxygen pressure is low, these associates decompose according to Equations 6 and 7, and one electron per tin ion is still donated to the conduction band.

$$\left[2Sn_{In}^{\bullet}O_i''\right]^x \rightarrow \frac{1}{2}O_2(g) + 2Sn_{In}^{\bullet} + 2e' \tag{6}$$

$$K_a = \frac{pO_2^{1/2}\left[Sn_{In}^{\bullet}\right]^2 n^2}{\left[2Sn_{In}^{\bullet}O_i''\right]^x} \tag{7}$$

One should expect that at higher oxygen pressures, a regime should be reached where the tin concentration should balance the concentration of the interstitial oxygens $Sn_{In}^{\bullet} = 1/2\left[O_i''\right]$, as pointed out by Ikuma and Murakami [45]. Since the oxygen interstitial concentration would be independent of the oxygen pressure in this regime, the oxygen vacancy concentration would also be independent of oxygen pressure, leading to a high oxygen dependence of $pO_2^{-1/4}$ for the electron population according to Equation 2. Instead a dependence of $pO_2^{-1/8}$ has been observed by Hwang *et al.* and by Frank and Köstlin [8, 37]. Frank and Köstlin concluded that this depencence also was related to the neutral Sn-oxygen interstial associates. At high oxygen pressures, these associates keep the electrons located, and the carrier concentration is no longer proportional to the tin concentration [8, 37].

Hwang *et al.* [8] presented the first calculated Brouwer diagram for ITO, depicted in Figure 3.7.

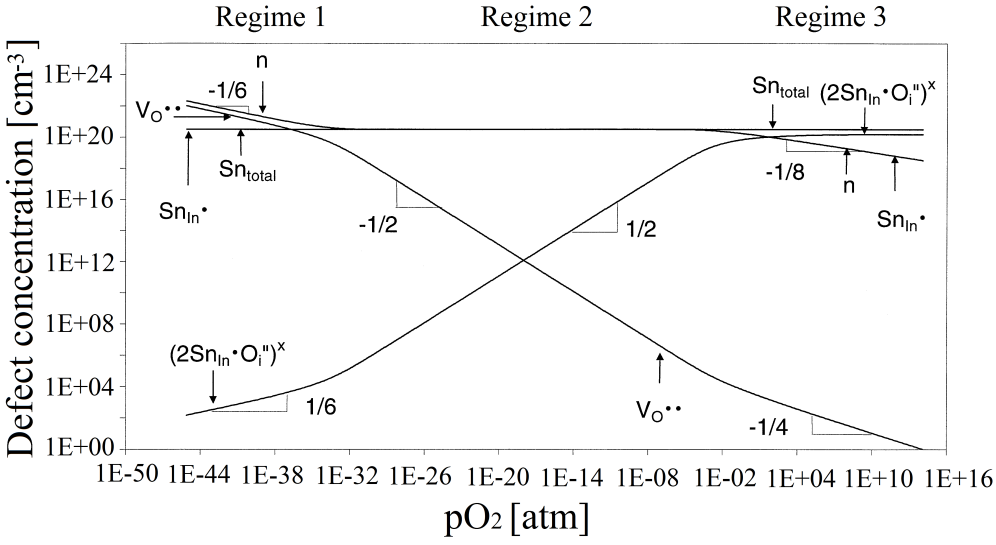

Figure 3.7: *Calculated Brouwer diagram of ITO with 1 cation% tin at 500°C by Hwang et al. [8] from 2000 showing the defect concentration and different defects in ITO as a function of oxygen partial pressure.*

As the carrier concentration varies, the mobility changes aswell, as shown in Frank and Köstlins diagram in Figure 3.8. The mobility increases with decreasing oxygen pressure (dashed lines) and, in the reduced state, approaches a limit. At constant pO_2, the mobility decreases with increasing tin doping concentration (continuous lines). Mobility and charge carrier concentration are linked to each other making it impossible to increase the conductivity above a certain limit. The mobility can be limited by scattering from different sources, such as phonons, grain boundaries and neutral and ionized point defects.

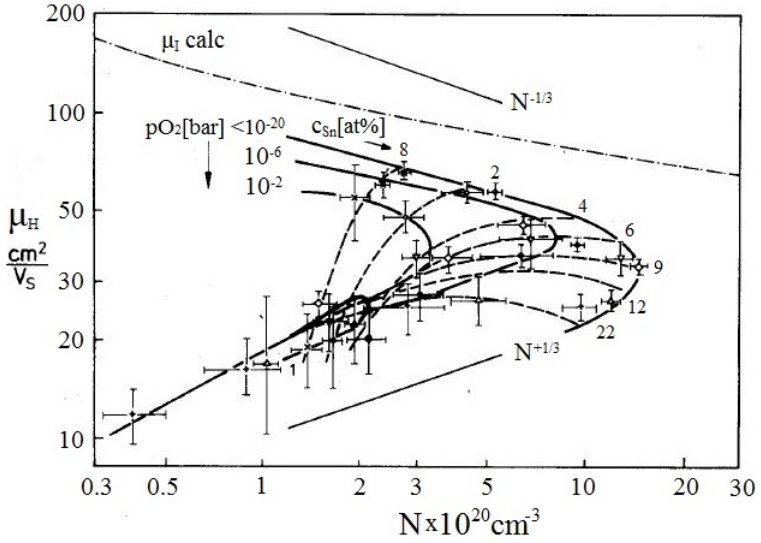

Figure 3.8: *Room-temperature Hall mobility vs. carrier concentration. — · —· mobility calculated for scattering by ionized impurities; - - - constant tin concentration, oxygen partial pressure varied; solid line: constant oxygen partial pressure, tin concentration varied [37].*

In general, both the mobility and the carrier concentration depend on the oxidation state and the dopant concentration in a rather complicated way [37]. Films prepared at low substrate temperatures tend to have mobility values of about 10-20 cm^2/Vs [46], whereas films prepared under optimized conditions attain values of 30-50 cm^2/Vs [47, 48] at carrier concentrations of N = 10^{21} cm^{-3}.

These discussions about charge carrier concentration and mobility lead to the electrical conductivity and resistivity of ITO. For dopipng of ITO to be successful, the dopant must be soluble in the host lattice, the donor level must be shallow in order to retain the large band gap and the dopant must not be compensated by an intrinnsic defect [49]. Alam *et al.* [4] presented

specific resistance data for ITO thin films of 250 nm, prepared by dip coating and heat treated in air at $260°C$ between each dipping, to tin concentration, given in Figure 3.9a. The resistance decreases at first due to the increase in charge carriers, donated from the tin ions. The resistance reaches its lowest value at 10 cation% Sn before it starts to increase due to tin associates which localises the electrons. Preparation at reducing conditions would prevent formation of tin associates by reducing the amount of interstitial oxygens. The resistivity would therefore become even smaller and the minimum would be shifted to higher tin concentrations. Increased annealing temperature also decreases the resistance, as shown in Figure 3.9b, with a minimum resistivity at around 600 $°C$.

Minimum specific resistivities of $\rho < 2 \cdot 10^{-4} \Omega cm$ have been reported at doping concentrations between 4 and 20 atom% Sn [37, 50, 51, 52, 53]. It has been reported by some authors that the electrical resistivity of ITO thin films decreases as the film thickness d increases. This is due to a larger cross-section for the electron to flow, but could also be explained by increased film homogeneity as the thickness increases, as described in Section 3.1.2. Films of thickness larger than $0.2 \mu m$ tend to be homogeneous [10, 37, 40].

Bandgap considerations

Figure 3.10 by Klein *et al.* [9] illustrates the important surface potentials and energy transitions of a generic n-type TCO. The fundamental bandgap (E_{g0}) sets the low energy limit of optical transparency, which should be $\geq$3 eV to ensure transparency throughout the visible spectrum. On the other hand, owing to high dispersion of the conduction band, degenerate doping can result in $\sim$5 eV or greater additional increase in the effective band gap [54], shown as ($E_F - E_{VBM}$) in Figure 3.10, where E_F is the Fermi level and E_{VBM} is the valence band maximum. This phenomenon is the well-

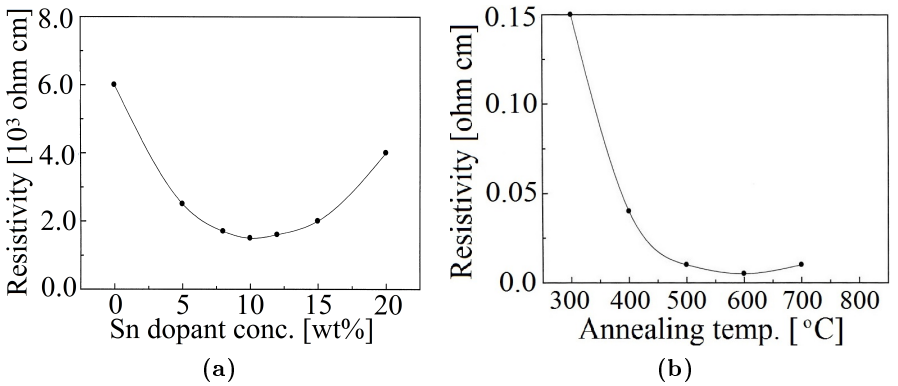

Figure 3.9: *(a) Resistivity of the ITO thin films (250 nm) annealed at 600°C as a function of tin dopant concentration [4]. (b) Resistivity of the ITO thin films as a function of annealing temperature [4].*

known Burstein-Moss shift of the Fermi level with doping. The Fermi level ($E_F - E_{VBM}$) therefore tells the amount of carrier doping that has been achieved. In general, the higher the Fermi level, the more conductive the TCO. Of course, at too high a doping level, free carrier absorption will shift the associated plasma frequency into the visible from the infrared and limit the optical transparency.

Despite of the remarkable optoelectronic properties of ITO, the physical mechanism responsible has not been topic for investigation for many researchers. Especially, the electronic structures near the bandgap which dominate the optoelectronic property, have not been studied well neither theoretically or experimentally. One of the reasons for this appears to be that the complex unit cell of indium oxide makes it difficult to perform theoretical electronic structure calculations.

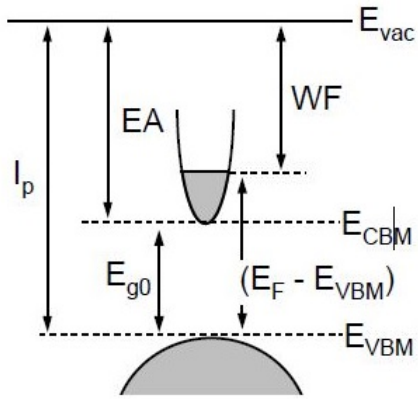

Figure 3.10: *Schematics of typical TCO band structure (a) and UPS spectrum (b); I_p, WF, E_A, E_{g0}, E_{vac}, E_{CBM}, E_{VBM}, and E_F denote ionization potential, work function (ϕ), electron affinity (χ), intrinsic band gap, vacuum level, conduction band minimum, valence band maximum, and Fermi level, respectively [9].*

Ambrosini *et al.* [33] reported that the localized doping levels of tin coalesce to form a dopant band which overlaps with the conduction band of the pure indium oxide. Electronic structure calculations by Myrasov and Freeman [8] showed that doping of In_2O_3 by Sn^{4+}, or oxygen vacancies, opened up a second bandgap (essential for transparency) between the conduction band and states at higher energy. In 2001 Odaka *et al.* [32] presented a work where electronic structure calculations of ITO resulted in a better understanding of the complicated band-structure. Their data showed that, when doping with tin, the overall features of the density of states (DOS) corresponding to the valence and conduction band of In_2O_3, were almost conserved except from the apparence of a new band below the valence band. This new band formed mainly from bonding states between Sn 5s-like and oxygen 2p-like states. Two other bands, of antibonding char-

acter, composed of Sn 5s-like states appeared in the conduction band and slightly disturbed this band. The Fermi level was situated in the lowest of these two bands. Since a tin atom has one valence electron more than an indium atom, substution of indium with tin will be expected to give one extra free electron in ITO. One can think of three scenarios for carrier generation in ITO. The first scenario is that the conduction band of indium oxide is constructed mainly from indium 5s-like stated and that tin atoms donate their electrons directly to this band. In this case, the electrical conductivity takes place in the indium 5s-like conduction band and there is no need of additional energy, such as light or heat, to create carrier electrons. The second scenario is that the tin ions form localised impurity bands below the conduction band. In this case, the electrons in the impurity bands cannot move, and for conduction to happen, some energy will be needed to excite these electrons to the conduction band of indium oxide. In this case we get a semiconductor behaviour with an activation energy. The third scenario is that the donor band, i.e., the Sn-like state itself becomes the conduction band of ITO. The investigations of Odaka *et al.* [32] showed that an intermediate case between the first and the third scenario appeared to occur in ITO. A substitutional tin atom donates an extra electron to the conduction band and this atom by itself forms a part of the conduction band. Since the symmetry of the donor band is the same as the original conduction band, the original conduction band does not seem to be significantly disturbed by the donor band.

The fundamental bandgap of In_2O_3/ITO was reported by Klein *et al.* [9] to 2.8 ± 0.2 eV. But it is widely known that highly degenerate thin films of ITO can exhibit band edge absorption in the range of 3.5–4.0 eV, which is much larger than the 2.8 eV fundamental bandgap. The Burstein-Moss shift alone cannot account for this large difference. One possible explanation

is the presence of an indirect gap that is significantly smaller than the direct band gap. However, recent density functional theory calculations have indicated that the energy difference between the overall VBM and the highest occupied level at the point is less than 50 meV [55]. X-ray emission spectroscopy results have also been consistent with a direct band gap for In_2O_3 [56]. Work by Walsh *et al.* [57] showed that the separation between weak and strong optical onsets (of ∼0.85–0.9 eV) arose from the fact that transitions from the highest valence bands into the conduction band are either symmetry-forbidden or have very low dipole intensity. Therefore, strong optical absorption in degenerate ITO films occurs above 3.65–3.70 eV and includes both the fundamental gap of 2.8 eV and the 0.85–0.90 eV separation described above.

3.1.4 Optical properties

Considering the previous Section 3.1.3, we understand that the electronic and optical properties of ITO and In_2O_3 are strongly related.

Good optical performance is crucial in evaluating the applicability of conducting oxide films. A high transparency for the ITO thin film in the visible region is required in applications with transparent electrodes for optoelectronic devices. ITO in thin film form exhibits 85-90 % transparency across the visible spectrum [33, 4], depending on the tin content. Figure 3.11a by Christian *et al. [58]* from 1982 compares the optical transmission spectra for ITO thin films with 5 weight% Sn deposited on glass in air with and without annealing. The figure shows that annealing increases the transmission. The work of Alam *et al. [4]* from 2000 confirmed this trend. An optical transmission spectrum of 10 weight% Sn-doped ITO thin films deposited on glass with a thickness of 250 nm is shown in Figure 3.11b with different annealing temperature. Increasing annealing temperature provides

improved optical transmission of the ITO film in the visible region, which can be attributed to increased structural homogeneity and crystallinity [4], and also a steeper optical absorption curve, which indicates a higher crystallinity and lower defect density near the band edge. The UV absorption edge is located at approximately 300 nm. The figure also shows that the transparency increases from 80 % at 400 nm to 85 % at 700 nm which is sufficiently high for the applications of a transparent conductor.

To obtain an adequate transmission of the ITO thin film, the thickness should be less than 150 nm [49]. But the film can not be to thin as this will lower the electrical conductivity of the film. There has to be a trade-off between the transparency and electrical conductivity when optimizing the properties of the TCO for specific applications.

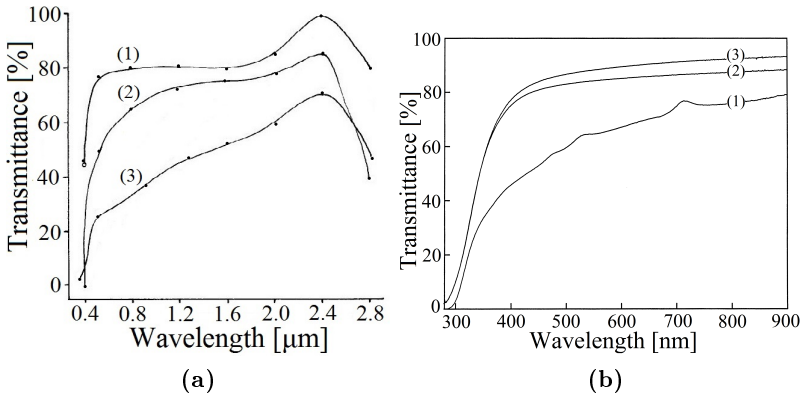

Figure 3.11: *(a) Comparison of transmission spectra for deposited films with soda-lime glass. All films were 250 Å thick deposited on soda-lime glass substrates. The curves show (1) bare soda-lime glass, (2) oxygen atmosphere deposited and annealed and (3) oxygen atmosphere deposited films* [58]. (b) *Optical transmission spectra of ITO films 250 nm with various annealing temperature (1) 400°C, (2) 500°C and (3) 600°C [4].*

3.2 Doping with terbium: Effects on the host

A good TCO must fulfill several requirements. The bandgap needs to be larger than 3.1 eV [9] to make the material transparent, and the charge carrier concentration needs to be high enough to give good electrical conductivity without compromising the mobility [37].

ITO is a semiconductor which combine good optical transparency and high electrical conductivity. The long-term goal with terbium-doping of this material is to introduce luminescent properties while retaining the remarkable properties of the host. To the authors knowledge, no research has been preformed on Tb-doped ITO, but one assumes that the introduction of this rare earth element will affect many of the properties of the host. Previous research on indium oxide and ITO doped with various rare earth elements, such as europium, erbium, praseodymium and terbium, are in many cases comparable to our situation, and the following discussions about these results can be closely related to the effects of terbium in ITO.

3.2.1 Crystal structure and phase composition

Previous research [14, 16, 59, 60, 61, 62] has shown that rare earth elements can be implemented successfully into In_2O_3 even at relatively high dopant concentrations without altering the crystal structure or phase purity. Xiao *et al.* [62] found that incorporation of 3 cation% europium into indium oxide gave the same phase purity and crystal structure as that of pure indium oxide. The observed d-spacing of the crystal structure was 0.413 nm, which is in good agreement with the lattice spacing for the (211) plane of cubic In_2O_3. Research [60, 14] has shown that ITO with around 10 cation% tin can retain phase purity when doped with 0.3 cation% $Eu^{3+}$and 1 cation% Nb^{3+}. In an unpublished thesis by Sunde [49] higher rare earth

concentrations were doped into ITO and In_2O_3. The results showed that nanocrystalline ITO powders with 5 and 10 cation% rare earth contained significant amounts of the rhombohedral In_2O_3 phase. Increasing calcination temperature from 400 to 600°C reduced the amount of the rhombohedral phase, and as high temperature as 1400°C almost eliminated the phase. For the thin films, no secondary phases could be seen even at as high dopant concentration at 10 cation% rare earth. The phase pure materials were assumed to be in a metastable state which allowed higher doping concentration than the solubility limit.

Rare earth elements oxidize with varying strength, but under suitable conditions, all the rare earths form sesquioxides, RE_2O_3 with a trivalent rare element in its ground state [63]. From neodymium onwards, with the exception of terbium, they occur naturally as sesquioxides, as the A-type hexagonal structure from lanthanum to neodymium, and as the C-type cubic bixbyite structure after terbium [64]. Terbium is an intermediate rare earth which can crystallise both as trivalent and fourvalent oxide. Petit *et al.* [63] suggested that its most stable form was as Tb_4O_7 with an oxidation number of $+3.5$, and that it could be oxidized to its fourvalent state as TbO_2 in high oxygen pressure, or reduced under oxygen deficient conditions to its trivalent state as the cubic bixbyite structure of Tb_2O_3, similar to In_2O_3 and ITO [63]. In fact, terbium oxides can crystallise in many different oxidation states describes as REO_x,$(1.5 \leq x \leq 2.0)$ [64]. The fourvalent Tb^{4+} is stabilised additionally by half-filled f-orbitals [63], but one should be aware that the cation/anion ratio is of equal importance when determining the structure of terbium oxide [64].

An illustration by the author of the relative stability of the dioxide versus the sesquioxide structures for ceria, praseodymium and terbium is seen in Figure 3.12. Terbium seems more stable as a sesquioxide compared to the

others. The trivalent terbium ions prefer the bixbyite structure and are only 15 % larger than the In^{3+} ions, and will therefore substitute the 8b positions and replace both indium ions and tin ions in these positions. Increasing the oxygen concentration above $10^{-5}bar$ the possibility of oxidizing the terbium to its fourvalent state is present [10].

When implementing rare earths into In_2O_3 and ITO, the lattice parameter shows shifting trends. Unpublished research by Sunde [49], where In_2O_3 and ITO thin films were doped with Eu^{3+} ions, showed that the lattice parameter decreased at small dopant concentrations towards a minimum at around 1 cation% and then started to increase as the dopant concentration increased further, as illustrated in Figure 3.13a. The figure shows that the lattice parameter has a minimum regardless of the In_2O_3 containing tin or not, but that it reaches its minimum at a lower rare earth concentration when the In_2O_3 is not doped with tin. The same thesis also found that preparing the same material as nanocrystalline powders, did not show the same trend, as depicted in Figure, mainly because of secondary phases forming during praparation. A similar trend for the lattice parameter has been observed for tin doping of In_2O_3, described in Section 3.1.1.

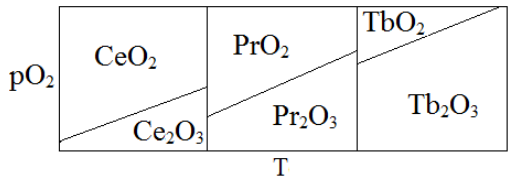

Figure 3.12: *Phase diagrams illustrating the relative stability of the dioxide and sesquioxide structures of Ce, Pr and Tb and thereby the relative stability of the trivalent and fourvalent oxidation states of the rare earth cations. Created with inspiration from Adachi et al. [64]*

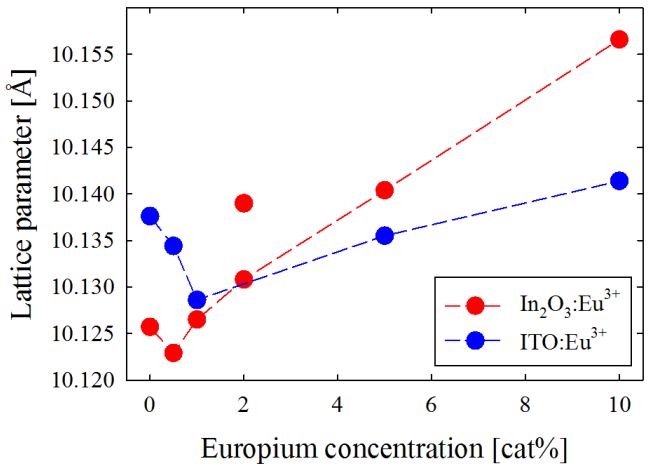

(a) *Thin films.*

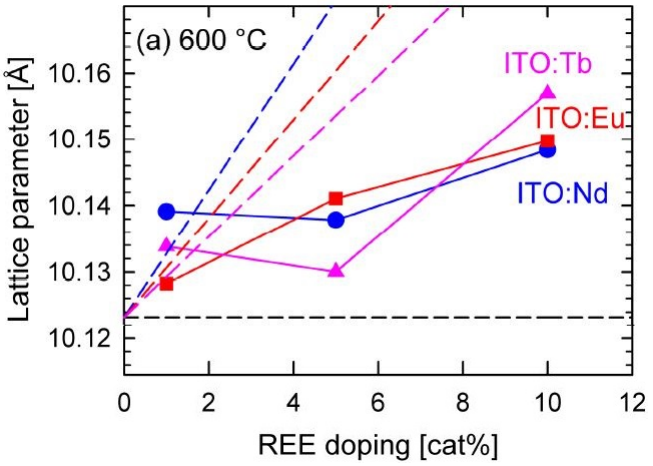

(b) *Nanocrystalline powders. The diagonal dashed lines are the lattice parameter according to Vegar's law with end values of 11.0770, 10.8660 and 10.7300 Å for Nd_2O_3, Eu_2O_3 and Tb_2O_3, respectively.*

Figure 3.13: *Lattice parameter of europium doped In_2O_3 and ITO thin films and nanocrystalline powders prepared at 600°C as a function of rare earth concentration [49].*

3.2.2 Nanostructure and microstructure

Research has found that the crystallite sizes of indium oxide and ITO nanoparticles are not affected significantly by incorporation of rare earth elements in the lattice structure. Xiao *et al.* [62] found that the average sizes of 3 cation% europium doped indium oxide nanoparticles heated at 600 °C decreased slightly compared to that of pure In_2O_3 counterparts ($\backsim$28 nm), which revealed that the incorporation of Eu^{3+} into In_2O_3 nanocrystals may restrained the nanocrystal growth to some extent. The $In_2O_3 : Eu^{3+}$ nanocrystals were irregular spheres with diameters ranging from 15 to 20 nm. Sunde *et al. [10]* showed the same results when preparing nanocrystalline In_2O_3 powders doped with Eu^{3+}.

3.2.3 Electrical conductivity

Ting *et al.* [61] reported results about Y^{3+} and Eu^{3+} co-doped ITO powders prepared in air. They found that the conductivity decreased slightly when increasing both the amounts of Y^{3+} and Eu^{3+}, as shown in Figure 3.14. Kim *et al.* [59] also reported a decrease in the electrical conductivity when doping In_2O_3 films with Er^{3+} prepared by sputtering. The films were deposited on quartz substrates and were annealed either in air ambient or in N_2/H_2 ambient. They found that Er-doping increased the resistivity by more than two orders of magnitude when prepared in both conditions, due mainly to a reduction of carrier concentration. This can be explained by the fact that Er oxidizes easily, and the oxygen atoms associated with Er atoms may fill oxygen vacancies in an indium oxide host during the sputtering. In fact, the Er-doped indium oxide films showed a reduced amount of n-type carrier concentration. Further, they reported that the increase in resistivity from the Er-doping could be much alleviated by postdeposition

annealing. In both ambient cases, the higher the annealing temperature was, the smaller resistivity increase was observed. Annealing in reducing ambient increased the carrier concentration dramatically (up to five orders of magnitude for the Er-doped samples case and three orders of magnitude for the undoped samples case). Oxygen desorption during the annealing in reducing ambient was believed to have contributed to this increase in carrier concentration. For the same reasons, terbium is also expected to decrease the charge carrier concentration when prepared or post-annealed in air.

Sunde [49] reported in an unpublished thesis that the effects were dependent on the material form of the rare earth doped ITO and In_2O_3 material. As described in Section 3.2.1, the work showed that the nanocrystalline thin films could be doped up to 10 cation% terbium without compromising the phase purity. The thermopower for the thin films, related only to the charge carrier concentration, appeared to vary so much that charge carrier concentration seemed to be of larger importance to the conductivity then the mobility, also implying that the mobility could be assumed constant.

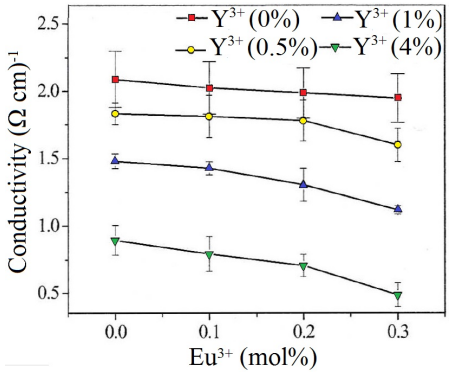

Figure 3.14: *Conductivity of the Eu^{3+}-Y^{3+} co-doped ITO pellets annealed in air at 600°C for 1 h as a function of different Eu^{3+}-Y^{3+} co-doping concentrations [61].*

When discussing the effect of terbium of the conductivity of the ITO host, it is reasonable to distinguish between the change in mobility and the change in charge carrier concentration. If substituted as a trivalent ion, terbium is expected to replace the 8b positions of indium oxide. Hence, the defect chemistry of the structure would not change, as illustrated by Kröger-Vink notation in Equation 8. In the presence of oxygen at high temperatures, the terbium would be oxidized to higher valence, and interstial oxygens would penetrate the structure to compensate the extra positive charge. This is illustrated by Kröger-Vink notation in Equation 9. When allowing oxygens to go into the structure the Tb^{4+} would localize the electrons and therefore reduce the number of charge carriers.

$$Tb_2O_3 \xrightarrow{In_2O_3} 2Tb_{In}^{x} + 3O_O^{x} \tag{8}$$

$$2TbO_2 \xrightarrow{In_2O_3} 2Tb_{In}^{\bullet} + 2O_O^{x} + O_i^{''} \tag{9}$$

Chatzichristodoulou *et al.* [65] reported results on the defect chemistry and thermomechanical properties of terbium and praseodymium doped ceria, $Ce_{0.8}Pr_xTb_{0.2-x}O_{2-\delta}$, which can be compared to ITO as a host. They found a relationship between the oxygen vacancy concentration, δ, and the partial pressure of oxygen, shown in Figure 3.15. At the insets of Figure 3.15a and 3.15b, where oxygen partial pressures and temperatures are low, Ce^{3+} is oxidized to Ce^{4+}, and it is observed that the Pr-rich compounds have a higher oxygen content (smaller oxygen nonstoichiometry) and are observed to absorb oxygen easier than the Tb-rich compounds with increasing P_{O_2}. In the intermediate part of the figures, the vacancy concentration is close to constant. The vacancy concentration of 0.10 corresponds to fourvalent cerium and trivalent dopants. When increasing the oxygen partial

pressure further, the Pr-rich compounds start to oxidize at higher oxygen pressures than the Tb-rich ones, which means that terbium is more stable as a trivalent ion than praseodymium is. This difference in stability of the different oxidation numbers with oxygen pressures for cerium, praseodymium and terbium was illustrated in Figure 3.12 in Section 3.2.1.

3.2.4 Optical properties

Li *et al.* [14] found that optical transmission of ITO thin films diminished only slightly when doping with Nb^{3+}. The same is expected for terbium doping of the ITO thin films. Sunde [49] also found that the optical transmission of the thin films was almost uaffected by rare earth doping due to high solubility in the host. If implemented completely into the crystal structure of ITO the material should interact with light in a similar manner. Small traces of impurities could scatter or absorb the light and reduce the transmittance.

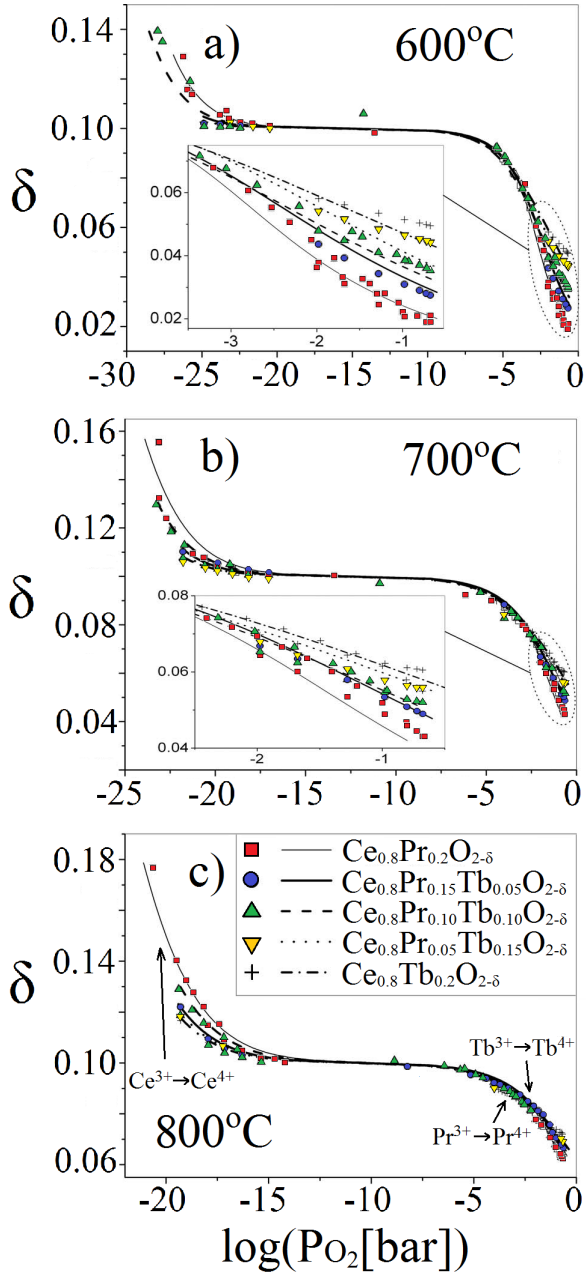

Figure 3.15: *Oxygen nonstoichiometry and fit of the δ-linear solution defect model for the compounds* $Ce_{0.8}Pr_xTb_{0.2-x}O_{2-\delta}$ *at a) 600, b) 700 and c) 800°C. Modified from Chatzichristodoulou et al.* [65].

3.3 Doping with terbium: Luminescence and upconversion

3.3.1 Luminescence

A phosphor, or luminescent material, is a material that emits light as a result of it absorbing energy. Luminescence is emission of light due to other causes than high temperature, such as electromagnetic radiation, beam of energetic electrons, current or voltage, mechanical energy and biochemical reactions in living organisms [21]. Phosphors are usually microcrystalline and transparent materials with a small amount of intentionally added impurity atoms, called activators, distributed homogeneously in the host. The luminescence processes can therefore be divided into those related to the host and those that occur around and within the activator. The latter process is often the dominant process.

The aim of this paper is not to give a detailed description of quantum mechanics related to the luminescence mechanisms, but to highlight the principles nescessary to understand one of the long-term goals of doping ITO with terbium. A luminescent material will only emit radiation when the exitation energy is absorbed. Absorption can occur as narrow lines or broad bands, either by the activator itself, by the host or by a sensitising atom depending on the allowed variation in exitation energy for the electrons. When a luminescent material absorbs energy, electrons in the activator are exited, and the transition from the initial ground state to the exited state can be either allowed og forbidden. Transitions between states that have the same parity (wavefunctions with the same symmetry), such as $f \rightarrow f$, are generally forbidden. Optical absorption transitions are strongly forbidden by the parity selection rule. If parity-forbidden transitions occur, the produced emmision is very weak. In practice, this means that electrons cannot redistribute themselves within the same orbital. This is known as

Laporte's selection rule. When a photon is emitted by a transitioning electron, the total momentum of the system must be conserved. The spin, or angular momentum, of a photon is 1, so when this photon is emitted, the total momentum of the system must also change by 1. This is often referred to as the spin rule [21].

Luminescent materials can be divided, depending on the decay time of exitation, τ, into fluorescent and phosphorescent materials. Fluorescence is a fast spin-allowed transition ($\triangle S = 0$) with a decay time less than 10 ms. Phosphorescence is a spin-forbidden transition ($\triangle S = 1$) with a decay time of more than 100 ms, in some cases up to a few hours. Practically, one can say that fluorescence is light emission during the time it is exposed to exiting radiation, while in phosphorescence, an afterglow is detectable by the human eye after cessation of exitation [21].

3.3.2 Principles of upconversion

Luminescent materials usually emit photons with lower energy than the excitation ions, and thereby follow Stokes law.

Coupled lanthanide and uranide f ions and transition-metal d ions, when embedded in host materials, may deviate from the above principle. Instead, they upconvert the frequency by anti-Stokes emissions with moderate to strong excitation intensities [17]. During upconversion, an ion is exited two or more times to a higher energy level than the exitation energy itself. It requires that the life time of the intermediate level is not too short, so that the excitation radiation will excite the ion more than once.

There are many possible upconversion processes with widely different conversion efficiencies, illustrated by the energy schemes for the six types of upconversion in Figure 3.16. From left to right the following processes are shown [15]:

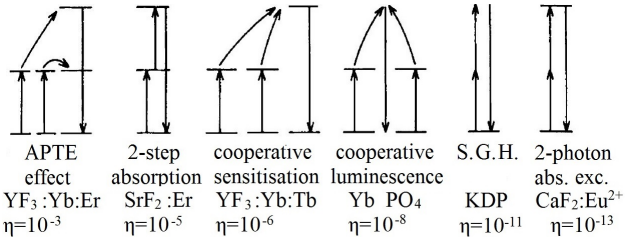

Figure 3.16: *Various two-photon upconversion processes with their relative efficiency in considered materials [17].*

- *Upconversion by energy transfer*, also called the Auzel APTE effect (for "Addition de Photon par Transferts d'Energie") or Energy Transfer Upconversion (ETU) [17]. An ion in the ground state A is exited to state B, and then transfers its excitation energy to another B state ion which is excited to state C and can now emit higher frequency.
- *Upconversion by two-step absorption*, also called multistep excitation due to classical excited state absorption (ESA) [17]. The same ion is excited two or more times until it reaches a higher state to emit from.
- *Upconversion by cooperative sensitisation* either between two ions or between a pair of ions and a third one. Two ions of the same type transfers excitation energy simultaneously to another ion which emits from a higher level.
- *Cooperative luminescence* where two A ions combine their excitation energy to one quantum which is emitted. The emitting level is only quasi-virtual.
- *Second harmonic generation*, also called frequency doubling, in which the frequency of the irradiated light is doubled without any absorption transition taking place.
- *Two-photon absorption* in which two photons are simultaneously absorbed without using any real intermediary energy level.

Luminescence can be limited by several factors which are mostly related to the concentration of the dopants and interactions between them, as listed under [20, 66].

- *Solubility in the host.* Above a certain dopant concentration, the dopants form clusters which may reduce the efficiency by either quenching as a result of ion-ion interaction, or by formation of unwanted compounds. This creates an upper boundary for dopant concentration. The sensitiser content is normally kept high (<20 mol%) in doubly or triply doped nanocrystals, while the activator content is relatively low (<2 mol%), minimizing crossrelaxation energy loss [62].
- *Multiphonon relaxation.* This only happens when a small number of phonons are required to bridge the energy gap between the upper and lower energy levels of the rare earth ion.
- *Ion-ion interactions* caused by nearby ions. If the ions are of the same kind, they can quench each other and create non-radiative transitions and loss. However, if they are of different kinds, it can create sensitisation of the rare earth and enhance the efficiency, which is an advantage.
- *Thermal/non-radiative transitions.* This may happen as a result of a long upper state lifetime where one of the two absorbed phonons are lost by thermal/non-radiative transitions or other unwanted transitions.

3.3.3 The rare earths and terbium

The rare earths, also referred to as lanthanides, comprise the series of elements in the sixth row of the periodic table stretching from lanthanum to ytterbium. These elements are characterised by partially filled 4f orbitals which are shielded from the surrounding matrix by the full $5s^2$ and $5p^6$ shells. This shielding provides similar ionic size and chemical properties throughout the series and their electronic levels are therefore relatively insensitive to the surrounding environment. When incorporated in crystalline or amorphous hosts, the rare earths usually exist as trivalent ions, but can occasionally be divalent or tetravalent ions. The trivalent ions all exhibit intense narrow-band intra-4f luminescence in a wide variety of hosts, and because of the $5s^2$ and $5p^6$ shielding, the rare earth ions exhibit radiative transitions resembling those of the free ions [20, 66]. The intra-4f transitions are, according to Laporte's selection rule, parity forbidden, but are made partially allowed by crystal field interactions mixing opposite parity wavefunctions. These elements are therefore phosphorescent with long lifetimes (often in the millisecond range) and narrow linewidths.

Tb^{3+} absorbs energy in the ultraviolet range in the form of 4f to 5d absorption bands. The dominant emitted radiation is green with wavelength of 545 nm, as seen in the energy splitting diagram for Tb^{3+}, given in Figure 3.17. Tb^{3+} has shown some good downconversion properties, but also upconversion has been detected for Tb^{3+} coupled with Eu^{3+} [15, 61] and with Yb^{3+} [67], as cooperative luminescence, where Tb^{3+} acts as a sensitiser for Eu^{3+} or Yb^{3+}. The efficiency for this process is somewhat lower than that of the APTE and ESA processes [15]. Sunde [49] observed no emissions for nanocrystalline In_2O_3 powders doped with terbium.

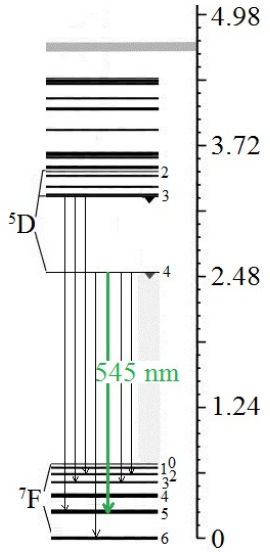

Figure 3.17: *Energy splitting diagram for the isolated Tb^{3+} ion showing dominant emittance of green light with wavelength 545 nm.*

3.3.4 ITO as a host for terbium

There are several requirements to consider when choosing a host for the phosphors. First and foremost, the phosphor should be soluble in the host lattice. Otherwise, precipitations will form which will quench or reduce the luminescence significantly. This is either caused by increased ion-ion interactions due to higer activator concentration or by the formation of compounds which are not optically active. Secondly, it is important that the lattice vibrations are not in the same order of magnitude as the exited energy states, as these will interfere and create non-emissive relaxation [49].

When the rare earths are trapped in host lattices, the matix effectively reduces the quenching of rare earth surface emission by shielding the rare earth ions present on the surface of the nanoparticles from the external

ligands [16]. This comes in addition to the above mentioned shielding from the outer $5s^2$ and $6s^2$ orbitals. The 4f energy levels are therefore shielded quite well from the surroundings. Still, the efficiency of the upconversion will depend strongly on the choice of host lattice. The host materials are generally required to match the structure and size of dopant ions and to have low phonon energies [66]. For this reason, oxides have traditionally been considered less suitable as host materials than fluorides, since oxides have stronger bondings, resulting in stronger vibrations and interactions with the dopant ion. This gives shorter lifetimes than in fluorides [15]. The more covalent bonding of oxides means that less energy is required to exite the electrons, and the energy transitions are lowered. This is known as the neuphelauxetic effect [15].

Strong interaction with the surroundings can result in Stark splitting, which broadens the levels as a result of low symmetry in the applied crystal field, such as in amorphous glass [20]. In crystalline hosts, the rare earths therefore prefer to substitute positions of high symmetry in the matrix [15, 20]. To the authors knowledge, there has not been conducted any research on the energy level splitting of Tb^{3+} in ITO as host material.

Several researchers [14, 59, 60, 61] have shown that rare earth doped conducting oxides hold considerable potential for physical applications since they may allow both electrical as well as optical excitation of the rare earth ions. This is due to several reasons. Firstly, their wide bandgap semiconductivity [3] results in negligble thermal quenching of the luminescence compared to semiconductors with narrower band gap, such as Si or GaAs [68], which means that luminescence can be maintained at higher temperatures. The high bandgap also opens up the possibility for host sensitisation, as illustrated in Figure 3.18. Here, the host absorbs energy across the bandgap and transfers it to one of the higher energy levels of Eu^{3+}. Secondly, the

electrical conductivity can be adjusted by controlling the stoichiometry of added dopants. Polycrystalline TCOs provide high conductivity, and even relatively high additions of rare-earth elements are not expected to deteriorate this property if the rare earths are substituted into the lattice structure.

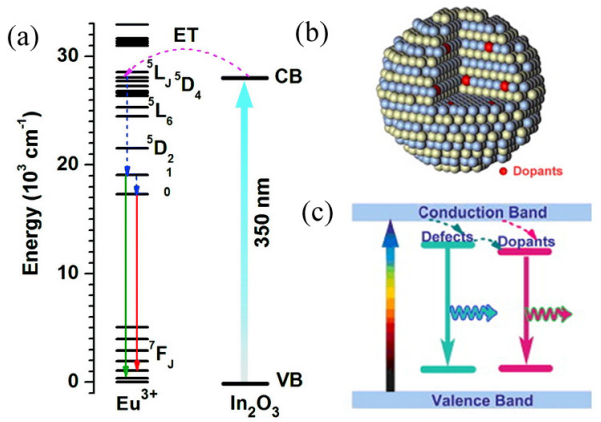

Figure 3.18: *Host sensitisation of a Eu^{3+} by absorption across the optical bandgap of In_2O_3.*

Ceria (CeO_2) is a crystalline mixed ionic electronic conductor with a fluorite structure quite reminiscent of the bixbyite structure of ITO. In ceria, all the oxygen positions are filled, whereas in bixbyite structure of ITO, one fourths of the oxygens are missing. Due to similar structures and cation sizes, ITO and ceria are expected to perform similarily as hosts for rare earths. The case of ceria doped with terbium and praseodymium was discussed in Section 3.2.3, showing that terbium can be implemented completely into the crystal structure [65]. Researchers have shown contradictory results on the luminescent properties of europium doped ceria. Wang *et al.*

[69] showed that europium was not efficient in increasing the photoluminescent properties of ceria nanocrystals, while Liu *et al.* [70] showed increased emission up to 1 mol% Eu^{3+} followed by a decrease due to concentration quenching. Kumar *et al.* [71] attributed these contradictory results to variations in defect concentration and the Ce^{3+}/Ce^{4+} ratio. Lowering the vacancy concentration and Ce^{3+} concentration, they managed to synthesise $CeO_2 : Eu^{3+}$ powders with increasing photoluminescence up to about 15 mol% europium.

Sunde [49] confirmed that also ITO was an appropriate host for rare earths, as the dopant could be implemented well into the structure without compromising the functional properties of the host. The results also showed luminescent properties when doping ITO powder with Eu^{3+}. No emission was detected for Tb^{3+} in ITO powders.

3.4 Preparation of nanocrystalline ITO by sol-gel

3.4.1 General principles of sol-gel techniques

The sol-gel technology was developed mainly during the last 40 years as an alternative for preparation of ceramics at considerably lower temperatures than the traditional high-temperature syntheses based on raw natural materials [72]. In this technique one starts off with an initial solution containing precursors in stoichiometric amounts. Treatment of this solution introduces different polymerization processes which lead to a gradual formation of a solid phase network. The initial solution undergoes several transformations during the process, including, gelling, drying, forming and calcination which result in formation of powders, fibers, coating, bulk monolithic products, thin film etc.

The sol-gel technology is a typical nanotechnology because all gel products may contain nanoparticles or are nanocomposites [73]. The large variety of products which can be produced from this technique illustrates its versatility and flexibility. Ferroelectrics, solid electrolytes, photocatalyst gels, coatings agains mist, hydrophilic aerogels, coatings for cars, microfilters and sensors are some products formed by sol-gel techniques [72].

Today, there exist a variety of chemical techniques to synthesise nanocrystalline thin films, such as reactive electron beam evaporation, DC magnetron sputtering, evaporation, reactive thermal deposition, spray pyrolysis, laser abliation and sol-gel deposition [4, 74]. Amongst these techniques, the sol-gel method seems to be the most attractive one due to easy coating of desired shape and area and easy control of the doping level, solution concentration, phase purity and homogeneity without using expensive and complicated equipment and precursors [4, 75].

3.4.2 The Pechini method and modifications for preparing ITO thin films

The prepared solution should be homogeneously mixed and remain stable. In some sol-gel methods, including the Pechini method, the solution stability is achieved by complexing the cations. The Pechini method, illustrated by chemical reactions in Figure 3.19, relies on the formation of complexes of alkali metals, alkaline earths, transition metals, or even non-metals with bi- and tridendate organic chelating agents such as citric acid [74]. A polyalcohol such as ethylene glycol is added to establish linkages between the chelates by a polyesterification reaction, resulting in gelation of the reaction mixture. The solvent is evaporated from the solution, resulting in a gel with strong covalent bonds [74], and the gel is then heated to obtain a nanocrystalline ceramic.

The Pechini method normally utilises acids with two or more carboxyl groups, so that a network can form between the adjacent acid molecules during complexation, as illustrated in Figure 3.19. A novel modified version of the Pechini method for preparing ITO, reported by Sunde *et al.* [10], replaces the citric acid, containing three carboxyl groups, with acetic acid which only has one carboxyl group. The synthesis starts by mixing relatively inexpensive precursor solutions of indium nitrate and tin acetate along with acetic acid as a complexing agent and ethylene glycol as gelation agent. The solution is further diluted in an aqueous solvent with 3 wt% polyvinyl alcohol (PVA). After drying, the gel is heated to initiate pyrolysis of the organic species, resulting in agglomerated submicron oxide particles [74].

The use of acetic acid with one carboxyl group would assumingly mean that proper gel formation is not possible in the system. The reason for this is in not yet fully understood, but one assumes that even if a network is not

formed, the bondings between the acid groups and the metal cations are strong enough to keep the cations apart. The effect of ethylene glycol in the solution is thereby also not understood well. Nonetheless, the aforementioned research by Sunde *et al.* has shown that the synthesis can provide high quality thin films and powders of high nanocrystallinity, homogeneity and phase purity.

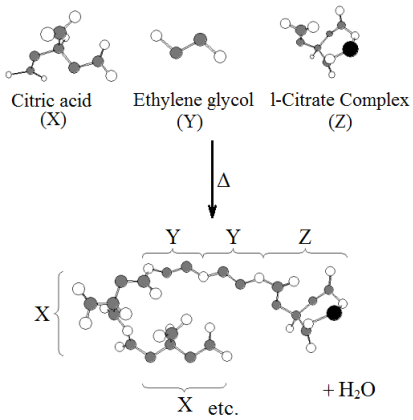

Figure 3.19: *Conceptual representation of the condensation between a metal cation, citric acid, and a polyol: the early stages of the Pechini method. Modified from Cushing [74].*

Preparation of nanocrystalline ITO thin films by spin coating

Spin coating is an easy and highly reproducible method where an excess of precursor solution is placed on a substrate and spun off by centripetal forces. The method is used to create a thin and even film, and the procedure can be repeated several times to obtain a multi-layer structure. An overview of the spin coating process is given in Figure 3.20.

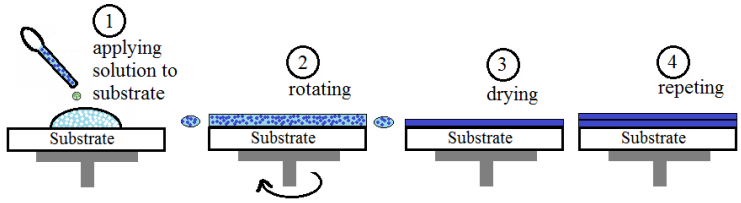

Figure 3.20: *The principle of the spin coating method for preparing thin films.*

To make defect free thin films, the following parameters are important in controlling the microstructure and thickness of the film [26]:

- Spin rate
- Viscosity of sol and wetting properties on the substrate
- Concentration of material-precursor
- Time between deposition of droplet and start of spinning
- pH of solution
- Number of layers deposited
- Age and stability of the sol
- Drying and heating program

4 Experimental work

4.1 Material synthesis

The synthesis route has been developed by Sunde *et al.* [10] for the preparation of nanocrystalline In_2O_3 and ITO thin films and powders. The preparation conditions for the thin films were chosen to give high conductivity and optical transmission. Previous research has shown that ITO thin films prepared at atmospheric oxygen partial pressures exhibit minimum specific resistance of $1.5 \cdot 10^{-3} ohm\,cm$ [4] when the tin concentration is around 10 cation% (11.5 cation% in a research by Alam *et al.* [4] and 12.5 cation% in a paper by Frank and Köstlin [37]). They also showed that a calcination temperature of the thin films of $600°C$ provided the lowest resistivities. The thin films exhibited good optical transmission of up to 93 % [4]. The tin concentration and the calcination temperature for the present work were chosen to 10 cation% and $530°C$, respectively. The thin films were annealed at reducing conditions, which would expect to give even higher conductivities than thin films prepared at atmospheric oxygen partial pressures.

Figure 4.1 provides a flow chart which summarises the process steps performed to prepare nanocrystalline powders and thin films. For preparation of ITO:Tb solutions, precursors of indium (III) nitrate hydrate ($In(NO_3)_3 \cdot xH_2O$, 99.9 %, Aldrich) and tin(II) acetate ($Sn(CH_3CO_2)_2$, 99.9 %, Aldrich) were used. Since indium nitrate hydrate is hygroscopic, an aqueous solution of indium nitrate hydrate was stardardised by a thermogravimetrical analysis where the solid was dissolved in deionized water and weighted. The doping element terbium was added to the mixture as terbium nitrate pentahydrate ($Tb(NO_3)_3 \cdot 5H_2O$, 99.9 %, Aldrich). Six different solutions were made. The desired ratio of tin compared to total amount of indium

and tin was 10 cation% Sn (cation% Sn = $\frac{n_{Sn}}{n_{Sn}+n_{In}}$). The desired ratio terbium relative to total amount of cations was 0.5, 1, 2, 5 and 10 cation% Tb (cation% Tb = $\frac{n_{Tb}}{n_{Sn}+n_{In}+n_{Tb}}$). A solution with 90 cation% indium and 10 cation% tin, without terbium, was also made as a reference composition. Acetic acid (AA) (CH_3COOH,p.a. Acros Organics) and ethylene glycol (EG) ($C_2H_4(OH)_4$, VWR) were used as the complexing agent and the esterification agent. They were added to give a molar ratio of 1:1.5 between the cations and the organic additives. The compositions for the different solutions are given in Table 4.1.

Finally, the solutions were diluted in a 1:1 volume ratio with a solution of 3 weight% PVA in deionized water in order to modify the concentration, viscosity, wetability and expansion differences between the substrate and the solution, so that the solutions could be used for spin coating of thin films as well as powder preparation. The cation concentration of the final solution was 0.2 M or 0.4 M. Details about the composition of each solution and the standardisation of the indium(III)nitrate precursor are given in Appendix A.

Table 4.1: *Compositions of the different solutions.*

Solution	**Amount In (cation%)**	**Amount Sn (cation%)**	**Amount Tb (cation%)**	**Total cation conc. [M]**
1	90	10	0	0.2
2	89.5	10.0	0.5	0.4
3	88.3	10.6	1.1	0.2
4	87.3	10.5	2.2	0.2
5	85.5	9.5	5.0	0.4
6	81.0	9.0	10.0	0.4

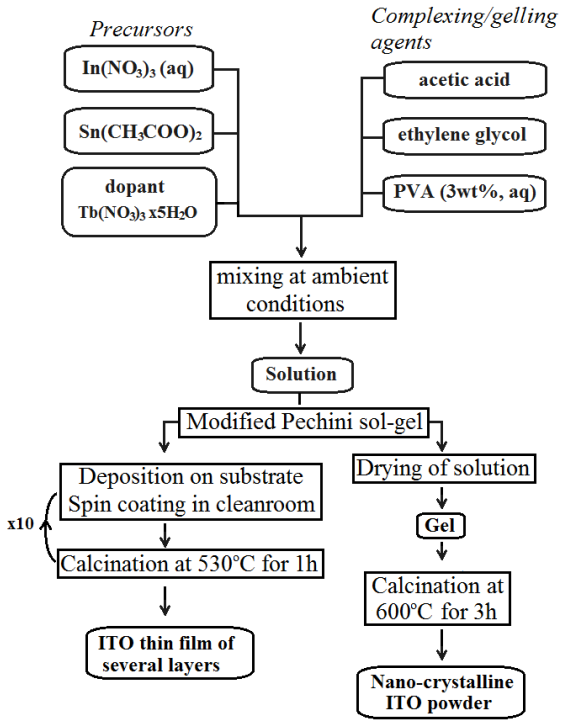

Figure 4.1: *Flow chart summarizing the process steps performed to prepare nanocrystalline ITO powder and ITO thin films.*

4.1.1 Preparation of nanocrystalline ITO thin films

The ITO thin films were deposited on square glass substrates (Menzel-Gläser, microscope slides) of 25x25 mm by spin coating. The substrates were washed with 5 % soap water, rinsed in ethanol and deionized water and dried with an airbrush prior to the deposition. The solution was applied to the substrates using a syringe with 0.2 μm filter to remove precipitates. The substrates were covered completely by applying a sufficient amount of solution, approximately 20 droplets. A spin coater (Laurell WS-400B-

6NPP-Lite Spinner) spun the substrates at 2500 rpm for 45 seconds. After short drying in air, the films were calcinated under vacuum (102 mbar, $10^{-10}atm \leq pO_2 \leq 10^{-5}atm$) in a rapid thermal process furnace (RTP, Jipelec JetFirst 200 Processor) at 530 $^{\circ}C$ for 1 hour. The chamber was purged with nitrogen gas before the onset of the vacuum, assuring an inert atmosphere. This procedure was repeated up to ten times in order to make multilayer thin films. Table 4.2 gives an overview of all the different thin films prepared from the solutions.

Table 4.2: *Overview of the prepared films and which solution that was used for the deposition.*

Solution	**3 layers**	**7 layers**	**10 layers**
ITO			x
ITO:0.5 cation% Tb	x	x	x
ITO:1.0 cation% Tb	x	x	x
ITO:2.0 cation% Tb			x
ITO:5.0 cation% Tb	x	x	x
ITO:10.0 cation%Tb	x	x	x

4.1.2 Preparation of nanocrystalline ITO powders

For the powder preparation, portions of the solutions were kept on a hot plate with a magnetic stirrer overnight in order to evaporate the solvent and transform the solutions into gels. Finally, the gels were ground lightly in an agate mortar and calcined for 3 hours at 600 $^{\circ}C$ in order to evaporate the organics and decompose the gels into nanocrystalline oxide powders.

4.2 Characterisation

The following techniques were applied in order to investigate the compositional, optical, electrical and structural properties of the thin films and powders.

4.2.1 X-Ray Diffraction Patterning

All of the synthesised powders were characterised by X-ray Diffraction Patterning (XRD) using a D8 Focus configured in θ-2θ mode (Bruker AXS) with $CuK\alpha_1$ radiation, while the thin films on glass substrates where characterised by grazing incidence X-ray Diffraction Patterning (GI-XRD) using a D5005 base goniometer configured in θ-θ mode (Bruker AXS) with $CuK\alpha_1$ radiation. The diffraction data from both powders and thin film were analysed using the software Diffrac.EVA version 2.1 (Bruker AXS), which provided phase composition and lattice structure, and by the software Diffrac.TOPAS version 4.2 for Rietveld refinements using the space group Ia3 in order to provide the lattice parameter of the crystal structure and the crystallite size from volume averaged column height calculated from the integral breadth, L_{vol-IB}.

The Rietveld refinement was performed using a hkl-phase in which the occupancy parameters are not included. This means that the software calculates the lattice parameters based only upon the position of the diffractogram reflections and not the shape of the reflections [76]. The shape is affected by the occupancy at each lattice plane and is therefore difficult to know precisely. The lattice parameter, crystallite size (both Gaussian and Lorentzian) and strain (both Gaussian and Lorentzian) were free parameters while the cell volume was held constant in the refinement.

4.2.2 Scanning Electron Microscopy

Scanning electron microscopy (SEM) using secondary electron emission was performed in a Zeiss Ultra 55 (Low Vacuum Field emission gun) for imaging the surfaces of a selection of the thin films at a nanoscale.

4.2.3 Ellipsometry

Ellipsometry is an optical technique which measures the change in polarization of elliptically polarized light when it travels trough a material, and was used to characterise the optical transmission of the thin films in the range of 0-1700 nm. The ellipsometry also gave the thicknesses of the thin films. The measurements were performed using a RC2 Ellipsometer (J. A. Wollam Co. Inc.). More detailed information about the technique and polarization is given i Appendix B, which summarizes some of the principles explained in a tutorial by Wollam Co. Inc. [77].

The absorption coefficients of the 10 layer thin films were calculated by a simplified relation neglecting the reflectance, as shown in Equation 10, where α is the absorption coeffisient, t is the thickness of the thin film and T is the transmission.

$$\alpha = \frac{1}{t} ln(T) \tag{10}$$

4.2.4 Conductivity measurements by the Van der Pauw method

Electrical conductivity measurements were performed on the thin films using an in-house built Van der Pauw apparatus. In order to remove edge effects from the spin coating, the substrates with the deposited thin films were cut into squares of approximately 12 $\times$ 12 mm from the center of the substrates. The electrical conductivity at ambient conditions was measured

for three, or in a few cases two, samples for each doping level of the rare earth element. The Van der Pauw method [78] utilises four platinum contact points placed quadratically apart on the thin film and measures electrical resistivity along the sides of the quadrate. These resistivities are referred to as $R_{AB,DC1}$, $R_{AC,DB1}$, $R_{AB,DC2}$ and $R_{AC,DB2}$ and can be averaged to the mean values $R_{AB,DC}$ and $R_{CA,BD}$. A correction factor, f, accounting for the geometric errors, is calculated by Equation 11. In the general case it is not possible to express the sheet resistance, ρ, explicitly by known functions, but the solution can however be written in the simplified form given in Equation 12. The sheet resistance is the specific resistance of the material, r, divided by the thickness of the film. For each sample, eight different configurations, where the current and voltage drop were measured in different directions and along different sides of the film, as shown in Figure 4.2, gave an average sheet resistance for the sample. Considering the values found for the thickness of the 10 layer thin films by ellipsometry, the specific resistance was calculated. In-situ conductivity measurements by the Van der Pauw method were also performed on the 10 layer ITO thin films where the films were heated in air at 300 ^oC for 6 hours and cooled to the initial temperature.

$$\frac{R_{AB,CD} - R_{BC,DA}}{R_{AB,CD} + R_{BC,DA}} = f \ \cosh^{-1}\left\{\frac{\exp\left(\ln 2/f\right)}{2}\right\} \tag{11}$$

$$\rho = \frac{\Pi d}{\ln 2} \ \frac{R_{AB,CD} + R_{BC,DA}}{2} \ f \tag{12}$$

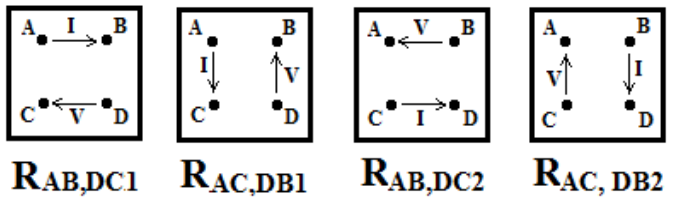

Figure 4.2: *Configuration of the contact points and current flow during conductivity measurements with Van der Pauw apparatus. Current (I) is measured along one side, and voltage (V) is measured along the other.*

4.2.5 Atomic force microscopy and luminescence microscopy

Atomic force microscopy (AFM) was performed in order to characterise the surface at a nanoscale, and luminescence microscopy was perfored to reveal if the samples showed any luminescent effects. These techniques proved to be quite difficult and non-conclusive due, amongst other reasons, to the nature of the thin films.

5 Results

5.1 Effect of terbium on the ITO host

5.1.1 Crystal structure and phase composition

The diffractograms for the nanocrystalline ITO thin films and the powders synthesised from the same solutions are given in Figure 5.1, along with a reference pattern for the bixbyite structure. The diffractograms show that all the thin films consist mainly of the cubic bixbyite polymorph with a negligable amount of impurities, as desired. The broad nature of the diffraction peaks imply that nanocrystalline ITO:Tb was formed.

Rietveld analysis provided the lattice parameters for synthesised thin films and powders. The lattice parameter for thin films of varying thickness are given in Figure 5.2a as a function of terbium concentration, and a clear trend can be observed. For the thin films prepared at reducing conditions, a decrease in lattice parameter can be seen at low terbium concentrations followed by a sudden shift at approximately 1 cation% Tb where the lattice parameter starts to increase as a function of terbium concentration. The slope lattice parameter seems decrease with terbim concentration. For the thin films of 10 layers post-annealed in air at 300^oC, a continuous increase in the lattice parameter can be observed as a function of terbium content, also with decreasing slope. One can also observe that the lattice parameter increases with the number of deposited layers, depicted as a function of number of deposited layers in Figure 5.2b. The lattice parameters for the nanocrystalline powders synthesised from the same solutions as a function of terbium concentration do not show such a clear trend, as seen in Figure 5.3. A more detailed overview of the refinement parameters and results to reveil the lattice parameters can be found in Appendix C.

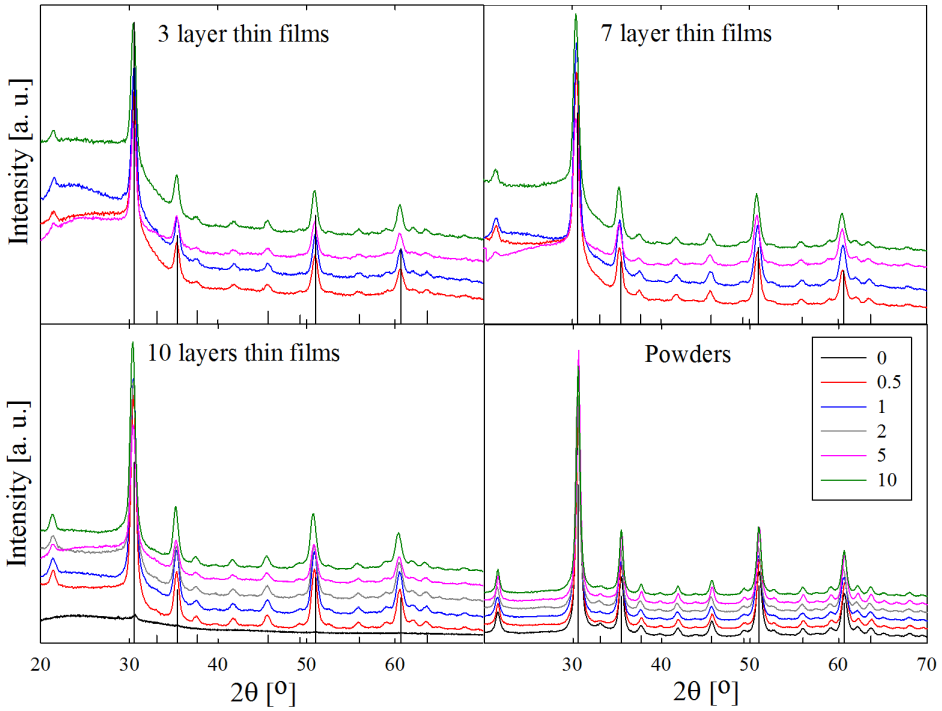

Figure 5.1: *Diffractograms for nanocrystalline thin films and powders of ITO:Tb. A reference pattern of the cubic bixbyite crystal structure (space group Ia3) for In_2O_3 is given as vertical lines. The legends refer to ITO:Tb thin films with 0 cation% (black line), 0.5 cation% (red line), 1 cation% (blue line), 2 cation% (grey line), 5 cation% (pink line) and 10 cation% (green line) terbium.*

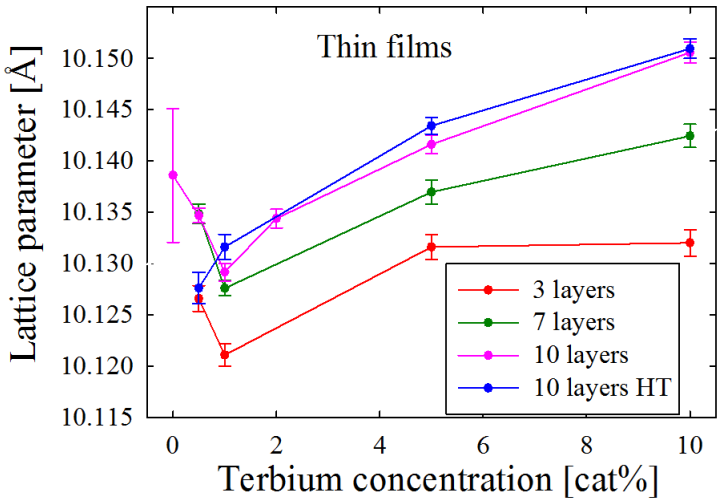

(a) *The legends refer to ITO:Tb thin films of 3 (red line), 7 (green line), 10 (pink line) as prepared deposited layers, and one post-annealed thin film of 10 (blue line) deposited layers.*

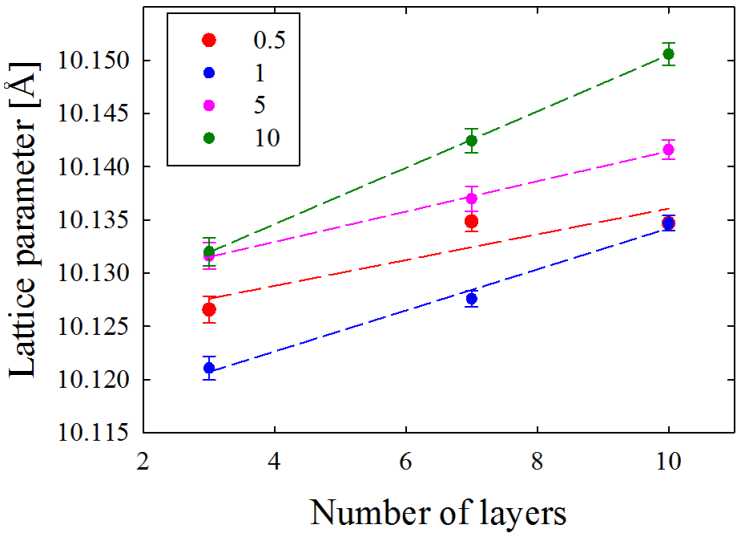

(b) *The legends refer to ITO thin films with 0.5 cation% (red line), 1 cation% (blue line), 5 cation% (pink line) and 10 cation% (green line) terbium.*

Figure 5.2: *Lattice parameters for the nanocrystalline ITO:Tb thin films and powders as a function of a) terbium concentration and b) number of deposited layers.*

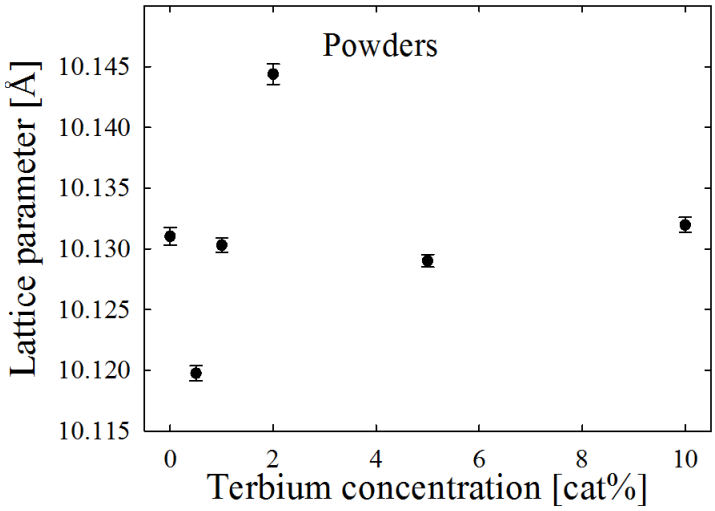

Figure 5.3: *Lattice parameters for nanocrystalline powders as a function of terbium concentration.*

5.1.2 Nanostructure and microstructure

The scanning electron microscopy (SEM) image of the surfaces of two thin films with 0.5 cation% terbium and 10 cation% terbium, respectively, given in Figure 5.4, show a smooth and homogeneous surface of spherical particles with relatively small grain size distribution. The mean grain size of the 0.5 cation% Tb thin film is 23 ± 1 nm, and the grain size for the 10 cation% Tb thin film is 22 ± 1 nm. The calculations for these grain sizes are given in Appendix D.

According to the Rietveld refinement, the crystallite size for the thin films does not depend on the terbium concentration, nor on the numbers of deposited layers, as can be seen in Figure 5.5a where the crystallite sizes for thin films of varying thickness are given as a function of terbium concentration. The value for the 10 layer ITO:Tb thin film with 0 cation%

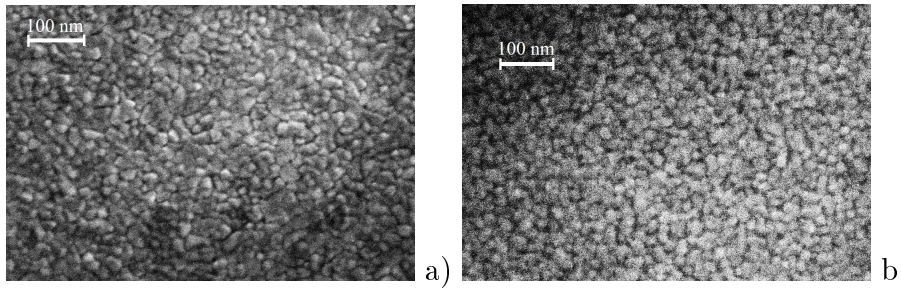

Figure 5.4: *Scanning Electron Microscopy image of the surface of 10 layer ITO:Tb thin films with a) 0.5 cation% Tb and b) 10 cation% Tb. The images show negligable change in the grain size size as a function of terbium concentration.*

terbium is somewhat lower than the other values, and is most likely due to poor quality of the corresponding X-Ray Diffractogram which was shown in Figure 5.1. The average crystallite size for the ITO:Tb thin films, excluding the outlier value of the 0 cation% Tb film, is 10 ± 1 nm. The crystallite sizes for the nanocrystalline ITO:Tb powders are more scattered than the corresponding values for the thin films, increasing from 10.4 nm to 14.6 nm, as shown in Figure 5.5b as a function of terbium concentration. The values for both the thin films and the powders are in the same order of magnitude as the grain sizes shown in Figure 5.4. A more detailed overview of the refinement parameters and results to reveil the crystallite sizes can be found in Appendix C.

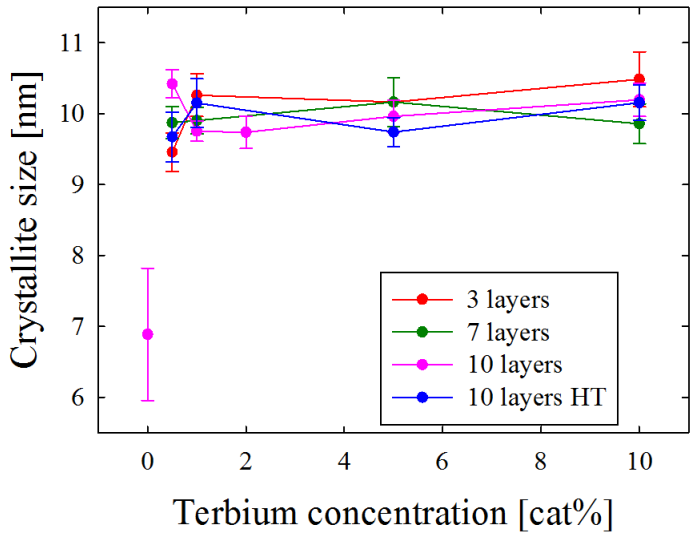

(a) *The legends refer to ITO:Tb thin films of 3 (red line), 7 (green line), 10 (pink line) as prepared deposited layers, and one post-annealed thin film of 10 (blue line) deposited layers.*

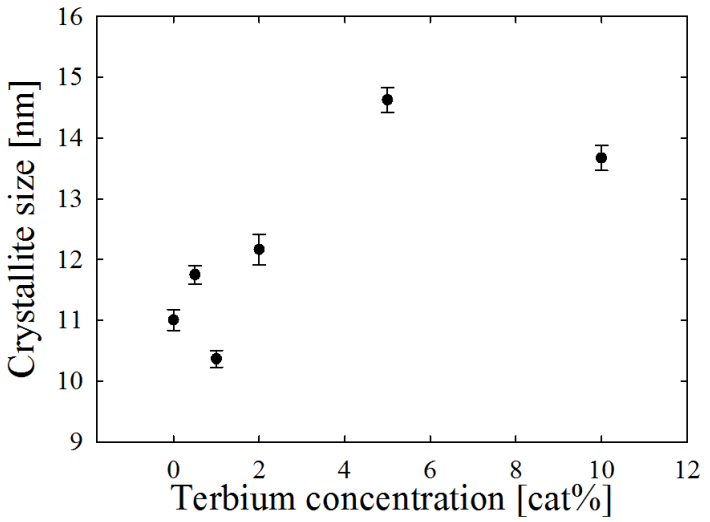

(b) *Crystallite sizes of the nanocrystalline ITO:Tb powders.*

Figure 5.5: *Crystallite size as a function of terbium concentration for (a) the nanocrystalline ITO:Tb thin films and (b) the nanocrystalline ITO:Tb powders. The crystallite sizes have been obtained by Rietveld refinement using the volume averaged column height calculated from the integral breadth, $L_{vol} - IB$.*

5.1.3 Electrical conductivity

The sheet resistances at ambient conditions of the ITO:Tb thin films of varying number of deposited layers as a function of the terbium concentration are given in Figure 5.6a. The sheet resistance increases as a function terbium concentration and there seems to be an increase in the slope. One can also see that the sheet resistance decreases as a function of the number of deposited layers and that the effect is more prominent at the higher terbium concentrations. The specific resistance for the 10 layer thin films as a function of the terbium concentration, calculated by dividing the sheet resistance by the thickness of the film, is given in Figure 5.6b. The figure shows a clear increase in specific resistance as the terbium concentration increases.

The thin films were also post-annealed in air ambient to 300^oC. The electrical conductivity curves for the 10 layer thin films for varying terbium concentrations as a function of the temperature during heating are given in Figure 5.7a. The conductivity increases for all the thin films at first, with a smaller increase as the terbium concentration increases. Line a in the figure marks a shift in the curvature, which occurs for all the thin films as the conductivity increases during the heating. A maximum conductivity, marked by line b in the figure, occurs for all the samples followed by a steep decrease in conductivity.

Figure 5.7b shows the electrical conductivity relaxation at a constant temperature of 300 ^oC given as a function of time. The conductivity decreases as a function of time for all the thin films and reaches the minimum conductivity in a shorter time when the terbium concentration is high.

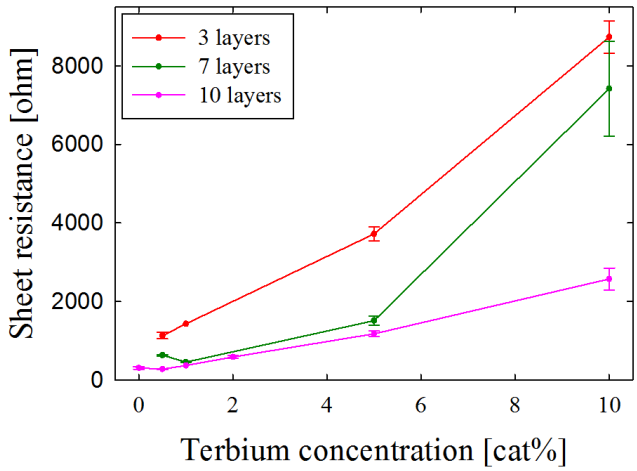

(a) *Sheet resistance at ambient conditions of ITO:Tb thin films of varying thickness as a function of the terbium concentration. The legends refer to ITO:Tb thin films of 3 (red line), 7 (green line), 10 (pink line) as prepared deposited layers.*

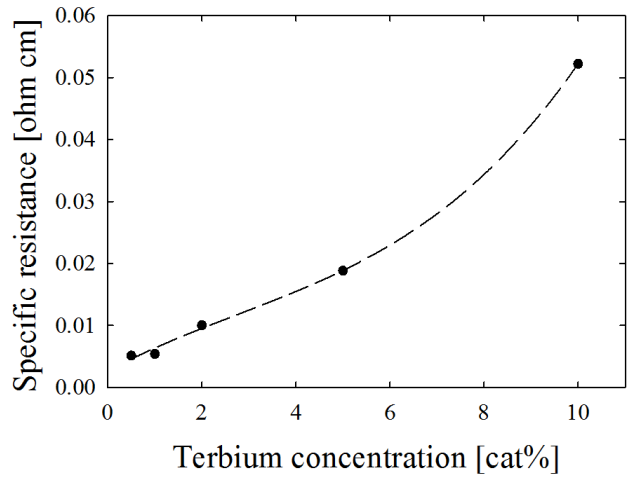

(b) *Specific resistance of the 10 layer ITO:Tb thin films as a function of the terbium concentration calculated from the sheet resistance multiplied by the thickness of the as prepared thin film.*

Figure 5.6: *Sheet resistance and specific resistance at ambient conditions of the as prepared ITO:Tb thin films as a function of terbium concentration.*

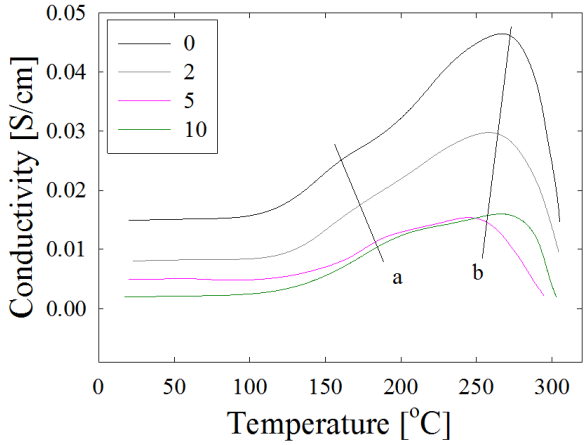

(a) *Electrical conductivity during heating up to 300°C in air of 10 layer ITO:Tb thin films of varying terbium concentration as a function the temperature.*

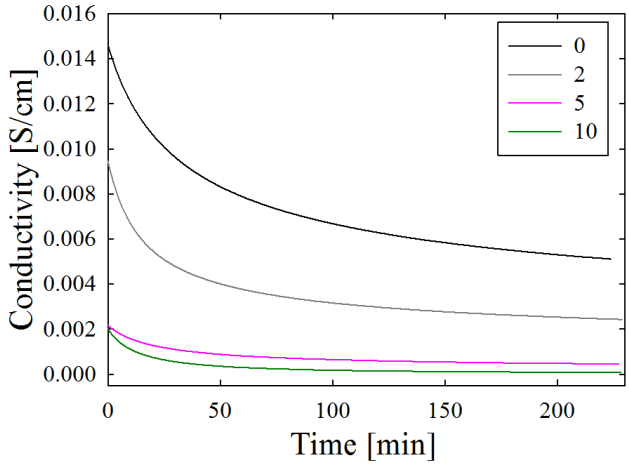

(b) *Electrical conductivity relaxation at 300°C for ITO:Tb thin films with varying terbium concentration as a function of time.*

Figure 5.7: *The legends refer to ITO:Tb thin films with 0 cation% (black line), 2 cation% (grey line), 5 cation% (pink line), 10 cation% (green line) terbium.*

5.1.4 Optical properties

The optical transmission curves for the as prepared 10 layer thin films of varying terbium concentration are given in Figure 5.8. The results have been obtained mainly by ellipsometry, but also by spectrophotometry for the thin films with 0, 1 and 2 cation% terbium.

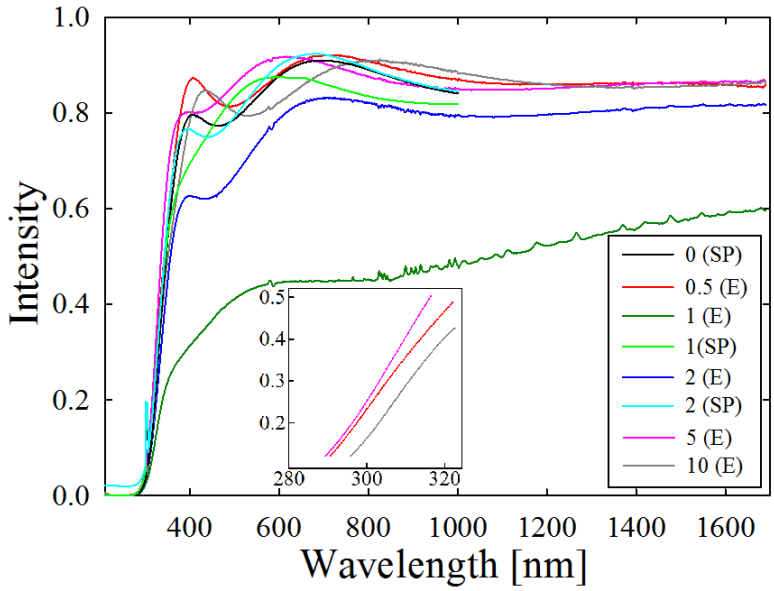

Figure 5.8: *Optical transmission of as prepared 10 layer ITO:Tb thin fims with varying terbium concentration for wavelengths in the range 0-1700 nm. The transmission was measured with ellipsometry for all the thin films, in addition to spectrophotometry for the 1 cation% Tb and the 2 cation% Tb sample. The legends refer to ITO:Tb thin films with 0 cation% (E) (black line), 0.5 cation% (E) (red line), 1 cation% (E) (dark green line), 1 cation% (SP) (light green line), 2 cation% (E) (dark blue line), 2 cation% (SP) (light blue line), 5 cation% (E) (pink line) and 10 cation% (E) (grey line) terbium, where E and SP are short for ellipsometry and spectrophotometry, respectively.*

The absolute values in this figure should not be considered reliable, because of the different measurement techniques and the poor reproducability of absolute values by both techniques.

Nonetheless, the relative trends are valid, such as the shape of the curves, confirmed for the samples which were measured by both techniques. The ellipsometry curves of the 1 and 2 cation% terbium samples provide very low absolute values, probably due to improper apparature parameters. For the other curves, the transmission is high, and up 92 % transmission in the visible spectrum and an absorption band edge around 350 nm. The transmission does not seem to be dependent on the terbium concentration. The maximum transmission along with the corresponding wavelengths for the thin films are given in Table 5.1.

A close-up of the curves from about 300 nm to 350 nm for the 0.5, 5 and 10 cation% terbium samples of 10 layers do not show any clear trend when it comes to the slope of the curves. For all the transmission curves measured by ellipsometry, one can observe a spike in the curves around the same wavelength. These spikes are only instrumental artifacts. The ellipsometry measurements showed that the optical bandgap of the thin films were independent of the terbium concentration and in the range of 3.2-3.6 eV.

Thicknesses of the thin films, which also were measured by ellipsometry, are also given in Table 5.1. The errors for these values are probably in the range of about 50 nm. The absorption coeffisients of the thin film, calculated from the thicknesses and maximum transmissions, are also given in the table. The absorption coefficient for the thin film with 2 cation% deviates from the other values.

Table 5.1: *Maximum optical transmission along with corresponding wavelengths for the 10 layer ITO:Tb thin films with various terbium concentrations measured by ellipsometry. The thicknesses measured by ellipsometry and the calculated absorption coefficients are also given. The error of the thicknesses is believed to be around 50 nm.*

Terbium conc. [cat.%]	**Wavelength [nm]**	**Max. transmission [%]**	**Thickness [nm]**	**Absorption coefficient**
0.5	728	92.1	184	$-1.9 \cdot 10^3$
1.0	620	-	146	-
2.0	714	83.1	171	$-4.7 \cdot 10^3$
5.0	612	92.0	160	$-2.3 \cdot 10^3$
10.0	825	91.1	203	$-2.0 \cdot 10^3$

5.2 Observations during the syntheses

During preparation of the ITO:Tb solutions, the solids dissolved easily in the aqueous solvent with acetic acid and ethylene glycol. The solutions seemed stable and homogeneous although some particles precipitated in all of the solutions only minutes after mixing. Nevertheless, it seemed like this amount remained constant after this first precipitation, and that the solutions were stable for several months after preparation. There was a slight difference in color nuance between the finished nanocrystalline powders. Figure 5.9a shows a 10 layer ITO:Tb thin film with 5 cation% terbium, while Figure 5.9b shows finished ITO:Tb powder.

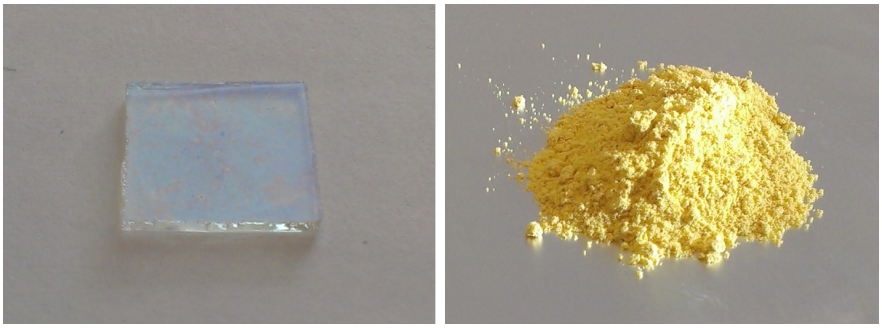

(a) *10 layer thin film.* **(b)** *Powder.*

Figure 5.9: *Prepared nanocrystalline ITO:Tb in powder form and as a thin film on glass substrate. The powder and the thin film contain 5 cation% terbium.*

6 Discussion

6.1 Effect of terbium on the ITO host

6.1.1 Crystal structure and phase composition

The X-ray diffractograms in Section 5.1.1 show that the modified Pechini sol-gel method adopted from Sunde *et al.* [10] can be used to synthesise nanocrystalline ITO (10 cation% tin) thin films and powders doped with terbium. All the thin films and powders seemed to be of high phase purity, with and without terbium, and no trace of impurities from the substrate was observed. But even though the diffractograms did not show any apparent secondary phases, a recent unpublished thesis by Sunde [49] showed that doping concentrations above 2 cation% terbium in ITO did cause formation of the rhombohedral ITO phase when prepared as nanocrystalline powders. The phase purity was much higher when the materials were prepared as thin films, with almost no trace of the secondary phase. The phase pure materials are assumed to be in a metastable state which allowed higher doping concentration than the solubility limit, in the same way as tin can be doped into In_2O_3 above the solubility limit. The broad nature of the diffractogram reflections indicated that the synthesised powders and thin films were all nanocrystalline. The large doping concentration of 10 cation% terbium exceeded the rare earth doping concentration of other researcher groups [14, 60, 61, 79], which have doped other rare earths into the ITO lattice. Our results therefore underlined their successful implementation of rare earths into ITO and showed that even higher amounts can be implemented than previously attempted.

The lattice parameter for the thin films showed some remarkable trends. A rather surprising trend was the shifting dependency of the lattice param-

eter on the terbium concentration. For the lower terbium concentrations, the lattice parameter decreased, followed by a sudden increase around 1 cation% terbium. The slope of the curves decreased as the terbium concentration increases, which indicated that the lattice parameter could reach a limiting value. These trends are not easily understood, but it is clear that there are several factors determining the lattice parameter of the crystal. Under the preparation conditions described in Section 4.1.1, the terbium is expected to be trivalent and to replace indium at its most symmetrical positions, i.e. the 8b positions, due to similar lattice structures [63, 64] and reduced Stark splitting in symmetrical positions [20]. The substitution of trivalent indium with trivalent terbium is not expected to affect the concentration of interstitial oxygens, so this would not affect the lattice parameter. But trivalent terbium has a larger ionic radius, 0.923, than trivalent indium, and a replacement of indium by terbium is expected to give an expansion of the lattice parameter. The increase in the lattice parameter at the higher terbium concentrations can be explained by this expansion. The decrease of the lattice parameter at the lowest terbium concentrations it not understood.

For the post-annealed thin films in air, we assume that that the terbium ions have been oxidized to its fourvalent state, based upon the research by Chatzichristodoulou [65] which showed that oxidation of terbium is prominent at ambient oxygen pressures at $600°C$. For these thin films, the lattice parameter increased continuously as the terbium content increased. We assume that tin is not affected by the conditions in our experiments, and is always fourvalent, but that terbium can be trivalent at inert conditions and fourvalent above a certain oxygen partial pressure (around $10^{-5}bar$). Tb^{4+} is alot smaller that Tb^{3+}, with a six-coordinated ionic radius of 0.76 Å [36], which is smaller than the replaced In^{3+} ion. As the terbium content in-

creases, more interstial oxygens will go into the structure to compensate the extra positive charge from the terbium ion, which would expect to expand the structure. This is called chemical expansion and is known for TCOs. This is similar to the increase when doping indium oxide with tin. It is difficult to distinguish and explain these effects, but they have been verified by Sunde [49] where both ITO and In_2O_3 were doped with Eu^{3+}, given in Figure 3.13a in Section 3.2.1. These results indicated that the shifting trend is not dependent on whether the lattice is doped with tin or not.

Another interesting trend is the lattice parameter's linear dependency on the number of deposited layers. Opposite results by Kim *et al.* [39] are not in compliance with our results. This mismatch could be due to difference in expansion coefficient between the glass substrates used in the present research and by Kim *et al.* In the present work, the glass substrates had an expansion coefficient of $9.06 \cdot 10^{-6}/^{\circ}C$ [80] which is higher than the expansion coefficient of the thin film of $7.2 \cdot 10^{-6}/^{\circ}C$ [39]. Kim *et al.* used a glass substrate with an expansion coefficient of $4.6 \cdot 10^{-6}/^{\circ}C$ [39], which is lower than that of the thin film. This creates opposite trends for the lattice parameters when the thickness changes.

Lattice parameters for the ITO:Tb powders did not show the same clear trend. The data seemed to follow the same trend as the thin films up to 2 cation% terbium and followed by an inflection point where the lattice parameters dropped to approximately the initial value. Based on the XRD, the powders seemed phase pure for all the compositions, but the data for the lattice parameter might indicate that secondary phases could have been formed for the nanocrystalline powders above 2 cation% terbium, but that the amounts or the crystallite sizes of the secondary phase were too small to be detected by the XRD measurements. The data showed some similarities to those of Sunde [49], which also showed an inflection point in

the lattice parameter for the nanocrystalline powders when the rare earth concentration was increased above 2 cation%. The same work also inferred that precipitaion of secondary phases in the nanocrystalline powders was the cause of the inflection point.

6.1.2 Nanostructure and microstructure

The smooth and homogeneous surfaces of the thin films shown in Figure 5.4 in Section 5.1.2 showed that the sol-gel method and deposition technique were appropriate for preparing the ITO:Tb thin films doped with terbium up to 10 cation%. The nanoscale grain size had low distribution and was nearly unaffected by the terbium concentration. Sunde *et al.* [10] implied that the grain size of the thin films reflected the thickness of each deposited layer and that each deposited layer was similar to a monolayer of particler, even after the final annealing step. The formation of sperical particles was also in compliance with previous results by Sunde *et al.* [10].

The crystallite sizes for the thin films of $10 \pm 1nm$ seem to be non-dependent on the terbium concentration. For the powders, the average crystallite size of $12 \pm 2nm$ was larger than that of the thin films, which could be due to the higher calcination temperature of the powders compared to that of the thin films. The values were more scattered, and is assumed to be related to precipitation of secondary phases. Previous research has reported that the crystallite size was fairly unaffected by rare earth doping [10, 62], both for nanocrystalline powders and thin films. Replacing In^{3+} with the isovalent Tb^{3+}, one would expect no change in the charge atmosphere in the lattice and hence the ionic mobility in the lattice is not affected either.

The grain sizes and the crystallite sizes are in the nanoscale and of same order of magnitude, which stresses the nanosize of the prepared samples.

6.1.3 Electrical conductivity

Electrical conductivity at ambient conditions

The research showed that the electrical conductivity of the ITO:Tb thin films decreased when doping with terbium. The decrease was very small at low terbium concentrations and increased with the terbium concentration. Overall, the change was not detrimental to the electrical properties of ITO as a transparent conducting oxide. The specific resistance for the as prepared 10 layer thin films at ambient temperatures given in Section 5.1.3, increased from $5.1 \cdot 10^{-3} ohm\,cm$ for 0.5 cation% terbium to $5.2 \cdot 10^{-2} ohm\,cm$ for 10 cation% terbium, which is an increase of only one order of magnitude. These values are within a reasonable distance from the resistivity values of ITO found by Alam *et al.* [4].

To understand why the electrical conductivity is affected by implementation of terbium, we need to consider the two factors determining the conductivity, namely the electrical mobility and the charge carrier concentration. When prepared under the inert conditions described in Section 4.1, the terbium ions are expected to be trivalent and to crystallise as an oxide as the cubic C-type bixbyite lattice structure with six-coordination as described in Section 3.2.3. When trivalent terbium is incorporated into the lattice of In_2O_3, it therefore does not provide an extra electron to the conduction band and does not contribute to the number of charge carriers in the material, as seen in Equation 20 in Section 3.2.3. Replacement of tin with terbium will therefore reduce the number of charge carriers. The terbium ions would also introduce impurity scattering, reducing the mobility [59].

The indium oxide structure was already doped with 10 cation% tin, approaching the solubility limit of tin in the lattice. Doping with terbium

would increase the total amount of doping elements in the structure [4, 34] and possibly enhance clustering of tin and/or terbium ions. This would reduce both the electrical mobility, by impurity scattering, and the charge carrier concentration, as the conduction electrons of tin would be localized. Sunde [49] showed that the mobility seemed almost independent on dopant concentration when doping ITO thin films with rare earths, indicating that the dominating cause of reduced conductivity was reduced number of charge carriers.

The sheet resistance for the as prepared 10 layer thin films decreased as a function of the number of deposited layers, as expected. With larger cross-section, the amount of mobile electrons is larger. Some of the decreased sheet resistance could also be due to reduced restraints from the substrate and higher homogeneity as the film thickness increases. This eases the electron flow and the conductivity increases.

Electrical conductivity during in-situ heating in air

The present work showed that heating the ITO thin films in air ambient up to $300°C$, caused an increase in conductivity up to a maximum during heating followed by a decrease to a value lower than the initial. The increased conductivity during the heating. During the heating, a shift in the curvature could be observed for all the samples, which was most likely due a flaw in the temperature measurements. After cooling to the initial temperature, the conductivity decreased to a value below the initial.

There are many factors determining the conductivity of the samples during the post-annealing. The first factor is the thermal exitation of electrons from the valence band to the conduction band. This behaviour is apparent in all semiconductors and is caused by higher electron energies. A second factor to consider is the tin. As the samples are heated while sur-

rounded by medium to high oxygen partial pressure, oxygen will penetrate the structure. Oxygen interstitials will by themselves reduce the charge carrier concentration and the mobility. Over a certain oxygen level, tin associates, or clusters, will form aswell. As described in Section 3.1.3, these associates will localise the tin electrons and prevent tin from donating an extra electron to the conduction band of In_2O_3. Thirdly, the terbium ions will be affected by the increased oxygen pressures as well. The terbium ions are expected to be trivalent at reducing conditions at room teemeperature. But as the temperature is increased, the terbium ions can react with the surrounding oxygen atmosphere and become oxidized to fourvalent. This will mostly affect the charge carrier concentration, as oxygens will go into the structure to compensate the extra positive charge, but also the mobility is expected to decrease because of change in the charge atmosphere. This reduces the carrier concentration and with it, the conductivity. The tin ions could also be oxidized, forming tin-oxygen associates trapping their conduction band electrons.

These oxidation effects result in a lower conductivity in the post-annealed state compared to the as prepared state. The relative difference between these states, taken at similar temperatures, is presented in Figure 6.1. As the terbium concentration increased, the reduction increased as well, from 69 % for the undoped ITO thin film to 99 % for the 10cation % terbium ITO thin film.

Both mobility and charge carrier conductivity will change when post-annealing the thin films in air, but as a first approximation the mobility is assumed constant when measured at the same temperature for both states. This is a valid assumption based on the results by Sunde [49] showing that the mobility seemed almost unaffected by the doping concentration. The change in carrier concentration between the as prepared and the post-

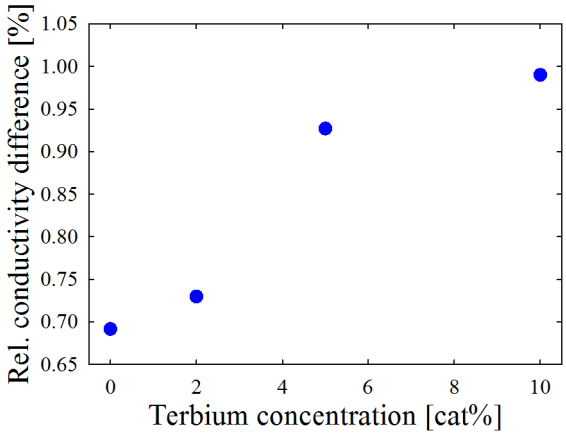

Figure 6.1: *Difference in electrical conductivity between the as prepared (reduced) thin films and the post-annealed (oxidized) thin films in air at 300°C.*

annealed state can then be calculated by the relation $\sigma = ne\mu_e$, where σ is the electrical conductivity, n is the number of charge carriers (in this case these are electrons), and μ_e is the mobility of the charge carriers. According to Sunde [49] we assume a mobility value of 15 cm^2/Vs.

The reduction of charge carrier concentration is a result of both oxidation of terbium ions and tin ions. These effects are difficult to distinguish, but considering the sample with no terbium, one can see how much the conductivity is affected by the tin ions and oxygen interstitials alone. Despite of substituting terbium into the structure, the tin concentration stays nearly unchanged; in fact it only changes by 1 cation% when doping with 10 cation% terbium. For simplicity, the tin concentration can therefore be assumed constant throughout the series of samples of varying terbium concentration. The 79 % decrease in the conductivity for the 0 cation% sample

can therefore be subtracted from the rest of the samples to be left with the influence of terbium oxidation on the conductivity reduction.

The change in carrier concentrations in total and due to oxidation of terbium along with the fraction of oxidized terbium ions to the initial amount of terbium ions in the reduced state are collected in Table 6.1. The reduction in conductivity increases in percentage with the terbium concentration, but since the initial conductivity was lower for the thin films with high terbium concentration compared to those with low terbium concentrations, the net number of charge carriers for the high terbium concentration samples were lower as well. The fraction of oxidized terbium ions seems to be decreasing with the terbium concentration. The reduction in the total number of charge carriers decreases with terbium concentration, which indicates that the initial reduction in conductivity by the doping itself is equally important as the post-oxidation on the reduced conductivity. The calculations can be found in Appendix E.

Table 6.1: *Change in carrier concentration between the as prepared and the post-annealed state in total along with total concentration of terbium ions for 10 layer thin films which have been heated in air up to 300 °C and cooled to the initial temperature. The mobility is assumed to be constant and equal to* $15cm^2/Vs$.

Total Tb conc. [cat.%]	**Rel. conductivity change [%]**	**Change in tot. no. of charge carriers** $[cm^{-3}]$	**Total number of Tb ions** $[cm^{-3}]$	**Fraction of Tb ions oxidized**
0	69	$4.3 \cdot 10^{15}$	0	0
2	73	$2.5 \cdot 10^{15}$	$6.2 \cdot 10^{22}$	$1.2 \cdot 10^{-8}$
5	93	$1.9 \cdot 10^{15}$	$1.5 \cdot 10^{23}$	$3.8 \cdot 10^{-9}$
10	99	$8.1 \cdot 10^{14}$	$3.1 \cdot 10^{23}$	$8.2 \cdot 10^{-10}$

A decrease in conductivity when doping with erbium was reported by Kim *et al.* [59] who attributed the reduction to reduced number of charge carriers due to the easy oxidization of Er^{3+} to Er^{4+}. Although the mobility most likely will decrease as the terbium concentration increases, mostly due to impurity scattering [59], one assumes that the reduction in charge carriers will affect the resistivity more. For each two Tb^{3+} that oxidizes to Tb^{4+}, one interstitial oxygen will go into the structure and the charge carrier concentration will decrease.

6.1.4 Optical properties

Overall, the optical transmissions of the 10 layer thin films were high enough to satisfy the requirements for a transparent conducting oxide and are in good agreement with the transparencies found previously by other reasearchers [3, 4, 44, 58]. The band absorption egde around 350 nm was also in compliance with previous research, giving a high transmission in the whole range of visible light. This indicates that terbium does not affect the transparency significantly even at as high dopant concentrations as 10 cation%. The absorption coefficient for the thin films did not show a trend. The scattering of the values is believed to be due to instrumental inaccuracy, and any trends would therefore be overshaddowed of this scattering. The measured optical bandgaps of the 10 layer thin films underpinned the good optical transparencies, which all were in the range of 3.2-3.6 eV. The values were in good proximity of the optical bandgap of ITO ($\sim$3.70 eV [9, 57]), which indicated that the optical properties were not effected by the terbium ions. This underlines the results from the crystal structure analysis which stated that there were negligible amounts of precipitations in the thin films.

6.2 Observations during synthesis and sources of error

The good stability and homogeneity of the solutions can be asserted to the solubility of the solids and proper choice of precursors and amounts. The precipitations in the solutions probably consisted of tin oxide, which formed both in the solid tin acetate before mixing and during the mixing of the solution. This, of course, affected the tin concentration of each solution, but we assume that the deviation is small enough not to compromise the results.

The variation in color nuance between the nanocrystalline powders are probably a result of variations in preparation conditions such as humidity, grinding pressure, time, temperature and general errors, giving different grain sizes, distributions and degree of agglomeration.

6.3 Outlook

No measurements of optical absorption or emission were performed during this work. Thus, no conclusions about the luminescent properties of terbium in ITO could be made. The optical transmission curves did not show any sign of absorption lines or bands, which indicated that the terbium ions could not be exited from the incident radiation. Absorption is the first step in luminescence and is nessescary to obtain luminescence. Absorption by terbium can be deteriorated if the ITO host has too high phonon energies or does not match the energy levels of the dopant. Thus, the bonding energies of the host will interact with those of the dopant ion, and this gives shorter lifetimes [66]. Sunde [49] showed that ITO powders doped with Eu^{3+} showed strong emissions, while ITO powder doped with Tb^{3+} did not. No measurements were conducted on the thin films, so no conclusions could be made whether or not the thin films would exhibit luminescent properties.

7 Conclusions

An environmentally friendly aqueous sol–gel process was successful in preparing nanocrystalline thin films and powders of ITO doped with the rare earth element terbium. The rare earth doping did not seem to significantly affect the functional properties of the ITO host. The films prepared by this simple and inexpensive technique had a high phase purity, while the powders seemed to contain some amounts of secondary phases based on measurements of crystallite size and lattice parameter. The specific resistance for the thin film with 0.5 cation% terbium was measured to $5.1 \cdot 10^{-3} \Omega cm$ and the one for the thin film with 10 cation% terbium was measured to $5.2 \cdot 10^{-2} \Omega cm$, which is an increase of about ten times and thereby not detrimental to the electrical properties of the TCO. Post-annealing of the prepared thin films in air up to $300°C$ showed a decrease in the conductivity, which became more prominent with the terbium concentration in the thin films. This decrease was attributed to oxidation of terbium and tin and thereby reduction of charge carrier concentration. The decrease in conductivity as a result of the doping by itself seemed to be equally important as the reduction caused by oxidation. The thin films showed good optical transmission in the visible area with an absorption band edge around 350 nm and a maximum optical transmission of about 92 %, independently on the terbium concentration. The SEM pictures of the surfaces of the ten layer thin films showed smooth and homogeneous surfaces of spherical particles with relatively small grain size distribution. The mean grain size of the 0.5 cation% Tb thin film was 23 ± 1 nm, and the grain size for the 10 cation% Tb thin film was 22 ± 1nm, indicating an independence of terbium concentration on the grain size. The crystallite size also seemed to be independent on terbium concentration. The lattice parameter for the thin films

showed some interesting trends. A decrease in the lattice parameter was observed for the lowest terbium concentrations followed by an increase with the terbium concentration. The latter effect was attributed to the larger size of Tb^{3+} compared to In^{3+}. The lattice parameter also increased with the number of deposited layers, probably due to strain between the substrate and the thin film.

Absorption and emission properties of the materials were not studied, and therefore no conclusions could be made about the luminescent properties of the ITO:Tb materials.

References

[1] D.S Ginley and C. Bright. Transparent Conducting Oxides. *MRS Bulletin*, 25:15–18, 2000.

[2] K. Bädeker. Über die elektrische Leitfähigkeit und die thermoelektrische Kraft einiger Schwermetallverbindungen. *Annalen der Physik*, 327:749–746, 1907.

[3] K. L. Chopra, S. Major, and D. K. Pandya. *Transparent Conductors - A Status Review*. Physics Department, Indian Institute of Technology, 1982.

[4] M. J. Alam and D. C. Cameron. Optical and Electrical Properties of Transparent Conductive ITO Thin Films Deposited by Sol-gel process. *Thin Solid Films*, 00:455–459, 2000.

[5] B. González, T. O. Mason, J. P. Quintana, O. Warschkow, D. E. Ellis, J.-H. Hwang, and J. D. Hodges, J. P. Jorgensen. Defect Structure Studies of Bulk and nano-Indium-Tin Oxide. *Journal of Applied Physics*, 96:3912–3920, 2004.

[6] C. G. Granqvist and I. Hamberg. Evaporated Sn-doped In_2O_3 Films: Basic Optical Properties and Applications to Energy Efficient Windows. *Journal of Applied Physics*, 60:122–159, 1986.

[7] C. G. Granqvist and A. Hultåker. Transparent and Conducting ITO films: New Developments and Applications. *Thin Solid Films*, 411:1–5, 2002.

[8] J.-H. Hwang, D. D. Edwards, Kammler D. R., and T. O. Mason. Point Defects and Electrical Properties of Sn-doped In-based Transparent Conducting Oxides. *Solid State Ionics*, 129:135–144, 2000.

[9] A. Klein, C. Körber, A. Wachau, F. Säuberlich, Y. Gassenbauer, S. P. Harvey, D. E. Proffit, and T. O. Mason. Transparent Conducting Oxides for Photovoltaics: Manipulation of Fermi Level, Work Function and Energy Band Alignment. *Materials*, 3:4892–4914, 2010.

[10] T. O. L. Sunde, E. Garskaite, B. Otter, H. E. Fossheim, R. Sæterli, R. Holmestad, M.-A. Einarsrud, and T. Grande. Transparent and Conducting ITO Thin Films by Spin Coating of an Aqueous Precursor Solution. *Journal of Materials Chemistry*, 22:15740–15749, 2012.

[11] T. Trupke, M. A. Green, and P. Würfel. Improving Solar Cell Efficiencies by Up-Conversion of Sub-Band-Gap Light. *Journal of Applied Physics*, 92:4117–4122, 2002.

[12] M. A. Green. Third generation photovoltaics: solar cells for 2020 and beyond. *Physica E*, 14:65–70, 2002.

[13] A. Shalav, B. S. Richards, and M. A. Green. Luminescent Layers for Enhanced Silicon Solar Cell Performance: Up-Conversion. *Solar Energy Materials and Solar Cells*, 91:829–842, 2007.

[14] S. Li, R. Ma, C. Ma, D. Li, Y. Xiao, L. He, and H. Zhu. Effect of thickness on optoelectrical properties of Nb-doped indium tin oxide thin films deposited by RF magnetron sputtering. *Optoelectronic letters*, 2013:198–199, 9.

[15] G. Blasse and B. C. Grabmeier. *Luminescent Materials*. Springer, 1994.

[16] V. Dutta, D. Sudarsan, P. Srinivasu, A.. Vinu, and A. . Tyagi. Indium Oxide and Europium/Dysprosium Doped Indium Oxide Nanoparticles: Sonochemical Synthesis, Characterization, and Photoluminescence Studies. *Journal of Physical Chemistry*, 112:6781–6785, 2008.

[17] F. Auzel. Upconversion and Anti-Stokes Processes with f and d Ions in Solids. *Chemical Reviews*, 104(1):139–173, 2004.

[18] P. Gibart, F. Auzel, J.-C. Guillaume, and K. Zahraman. Below Bandgap IR Responce of Substrate-Free GaAs Solar Cells Using Two-Photon Up-Conversion. *Journal of Applied Physics*, 35:4401–4402, 1996.

[19] T. Trupke, A. Shalav, B. S. Richards, P. Würfel, and M. A. Green. Efficiency Enhancement of Solar Cells by Luminescent Up-Conversion of Sunlight. *Solar Energy Materials and Solar Cells*, 90:3327–3338, 2006.

[20] A. J. Kenyon. Recent Developments in Rare-Earth Doped Materials for Optoelectronics. *Progress in Quantum Electronics*, 26:225–284, 2002.

[21] M. Nazarov and D. Young Noh. New Generation of Europium and Terbium Activated Phosphors. In *New Generation of Europium and Terbium Activated Phosphors*. Pan Standford Publishing, 2011.

[22] F. Kurdesau, G. Khripunov, A. F. Cunha, M. Kaelin, and A. N. Tiwari. Comparative Study of ITO Layers Deposited by DC and RF Magnetron Sputtering at Room Temperature. *Journal of Non-Crystalline Solids*, 2006.

[23] F. O Adurodija, H. Izumi, T. Ishihara, H. Yoshioka, , M. Motoyama, and K. Murai. Pulsed Laser Deposition of Crystalline Indium Tin Oxide

Films at Room Temperature by Substrate Laser Irradiation. *Journal of Applied Physics*, 39:377–379, 2000.

[24] M. Ait Aouaj, R. Diaz, A. Belayachi, F. Ruedab, and M. Abd-Lefdil. Comparative Study of ITO and FTO Thin Films Grown by Spray Pyrolysis. *Material Research Bulletin*, 44:1458–1461, 2009.

[25] T. Maruyama and K. Fukui. Indium Tin Oxide Thin Films Prepared by Chemical Vapour Deposition. *Thin Solid Films*, 203:297–302, 1991.

[26] D. W. Richerson. *Modern Ceramic Engineering - Properties, Processing and Use in Design*. CCR Press, USA, 2th edition edition, 2006.

[27] Dinguo Chen. Anti-reflection (AR) coatings made by sol-gel processes: A review. *Solar Energy Materials and Solar Cells*, 68:313–336, 2001.

[28] J. P. Cronin, D. J. Tarico, J. C. L. Tonazzi, A. Agrawal, and S. R. Kennedy. Microstructure and Properties of Sol-Gel Deposited WO_3 Coatings for Large Area Electrochromic Windows. *Solar Energy Materials and Solar Cells*, 29:371–386, 1993.

[29] T. Ogi, L. B. Modesto-Lopez, F. Iskandar, and K. Okuyama. Fabrication of a Large Area Monolayer of Silica Particles on a Sapphire Substrate by a Spin Coating Method. *Colloids and Surfaces A: Physicochemical Engineering Aspects*, 297:71–78, 2007.

[30] C. Brechignac, P. Houdy, and M. Lahmani. *Nanomaterials and Nanochemistry*. Springer, Berlin, Germany, 1th edition edition, 2006.

[31] B. Otter. Chemical Solution Deposition of Transparent Conducting Oxide Thin Films. Master's thesis, University of Applied Sciences, Northwestern Switzerland, 2011.

[32] H. Odaka, Y. Shigesato, T. Murakami, and S. Iwata. Electronic Structure Analyses of Sn-doped In_2O_3. *Journal of Applied Physics*, 40:3231–3235, 2001.

[33] A. Ambrosini, A. Duarte, K. R. Poeppelmeier, M. Lane, C. R. Kannewurf, and T. O. Mason. Electrical, Optical, and Structural Properties of Tin-Doped In_2O_3-M_2O_3 Solid Solutions (M=Y, Sc). *Journal of Solid State Chemistry*, 153:41–47, 2000.

[34] W. Heward and D. Swenson. Phase equilibria in the pseudo-binary In_2O_3-SnO_2 system. *Journal of Materials Science*, 42:7135–7140, 2007.

[35] Y. G. Park, K. H. Seo, J. H. Lee, J. J. Kim, S. H. Cho, C.J. O'Connor, and J. S. Lee. Phase Transformation Behavior of Nanocrystalline ITO Powders during Heat-Treatment: Oxygen Partial Pressure Effect. *Journal of Electroceramics*, 13:851–855, 2004.

[36] R. D. Shannon and C. T. Prewitt. Effective Ionic Radii in Oxides and Fluorides. *Acta Crystals*, 25:925–946, 1969.

[37] G. Frank and H. Köstlin. Electrical Properties and Defect Model of Tin-Doped Indium Oxide Layers. *Applied Physics A*, 27:197–206, 1982.

[38] J. J. C. Fan and J. B. Goodenough. X-ray Photoemission Spectroscopy Studies of Sn-doped Indium-Oxide Films. *Journal of Applied Physics*, 48:3524, 1977.

[39] H. Kim, J. S. Horowitz, G. Kushto, A. Piqué, and Z. H. Kafafi. Effect of film thickness on the properties of indium tin oxide thin films. *Journal of Applied Physics*, 88:6021–6025, 2000.

[40] E. Guo, H. Guo, H. Lu, K. Jin, M. He, and G. Yang. Structure and Characteristics of Ultrathin Indium Tin Oxide Films. *Applied Physics Letters*, 98:1–3, 2011.

[41] J. H. W. De Wit. Electrical properties of In_2O_3. *Solid State Chemistry*, 8:142–149, 1973.

[42] J. H. W. De Wit. High temperature behaviour of In_2O_3. *Solid State Chemistry*, 13:192–200, 1975.

[43] J. H. W. De Wit. Structural aspects and defect chemistry in In_2O_3. *Solid State Chemistry*, 20:143–148, 1977.

[44] H. Köstlin, R. Jost, and W. Lems. Optical and Electrical Properties of Doped In_2O_3 Films. *Physics Status Solidi*, 29, 1975.

[45] Y. Ikuma and T. Murakami. Oxygen Tracer Diffusion in Polycrystalline In_2O_3. *Journal of ELectrochemical Society*, 143:2698, 1996.

[46] H. Hoffmann, J. Pickl, M. Schmidt, and D. Krause. Hf-Sputtered Indium Oxide Films Doped with Tin. *Applied Physics*, 16:239–246, 1978.

[47] J.C.C. Fan and F.J. Bachner. Properties of Sn-Doped Films Prepared by RF Sputtering. *Journal of Electrochemical Society*, 122:1719–1725, 1975.

[48] R. Groth. Untersuchungen an halbleitenden Indiumoxydschichten. *Physics Status Solidi*, 14:69–75, 1966.

[49] T. O. L. Sunde. Aqueous sol-gel processing of transparent conducting rare earth doped indium tin oxide. June 2013.

[50] O. P. Agnihotri, A. K. Sharma, B. K. Gupta, and R. Thangaraj. The Effect of Tin Additions on Indium Oxide Selective Coatings. *Journal of Applied Physics*, 11:643–648, 1978.

[51] D. B. Fraser and H. D. Cook. Highly Conductive, Transparent Films of Sputtered $In_{2-x}Sn_xO_{3-y}$. *Journal of ELectrochemical Society*, 119: 1368–1374, 1972.

[52] H. W. Lehman and R. Widmer. Preparation and Properties of Reactively Co-Sputtered Transparent Conducting Films. *Thin Solid Films*, 27:359–368, 1974.

[53] J. L. Vossen. Control of Film Properties by RF-Sputtering Techniques. *Journal of Vacuum Science and Technology*, 8:12–30, 1971.

[54] I. Hamberg, C. G. Granqvist, K.-F. Berggren, B. E. Sernelius, and L. Engström. Band-gap widening in heavily Sn-doped In_2O_3. *Physical Review B*, 30:3240–3249, 1984.

[55] P. Erhart, A. Klein, R. G. Egdell, and K. Albe. Band structure of indium oxide: Indirect versus direct band gap. *Physical Review B*, 75: 1–4, 2007.

[56] L. F. J. Piper, A. DeMasi, S. W. Cho, K. E. Smith, F. Fuchs, F. Bechstedt, C Körber, A. Klein, D. J. Paine, and R. G. Egdell. Electronic structure of In_2O_3 from resonant X-ray emission spectroscopy. *Applied Physics Letters*, 94:1–3, 2009.

[57] A. Walsh, J. L. F. Da Silva, S.-H. Wei, C. Körber, A. Klein, L. F. J. Piper, A. DeMasi, K. E. Smith, G. Panaccione, P. Torelli, D. J. Payne,

A. Bourlange, and R. G. Egdell. Nature of the Band Gap of In_2O_3 Revealed by First-Principles Calculations and X-Ray Spectroscopy. *Physical Review Letters*, 100:1–4, 2008.

[58] K. D. J. Christian and S. R. Shatynski. Optical Properties of thin In-Sn Oxide Films. *Applications of Surface Science*, 15:178–184, 1982.

[59] H. K. Kim, C. C. Li, G. Nykolak, and P. C. Becker. Photoluminescence and electrical properties of erbium-doped indium oxide films prepared by rf sputtering. *Journal of Applied Physics*, 76:8209–8211, 1994.

[60] P. Psuja and W. Strek. Preparation of europium doped tin oxide, indium oxide and ITO nanocomposites. *Nanophotonic Materials*, 6639: 1–10, 2007.

[61] C.-C. Ting, C.-H. Tsai, Y.-C. Chien, and C.-T. Yu. Enhanced Red Light Photoluminescence of the Europium and Yttrium Co-Doped ITO Powders. *Journal of the Electrochemical Society*, 159:400–406, 2012.

[62] Q. Xiao, Y. Liu, L. Liu, R. Li, W. Luo, and Chen X. Eu^{3+}-Doped In_2O_3 Nanophosphors: Electronic Structure and Optical Characterization. *Journal of Physical Chemistry*, 114:9314–9321, 2010.

[63] L. Petit, A. Svane, Z. Szotek, and W. M. Temmerman. Electronic Structure of Rare Earth Oxides. *Topics of Applied Physics*, 106:331–343, 2007.

[64] G.-Y. Adachi and N. Imanaka. The Binary Rare Earth Oxides. *Chemical Reviews*, 98:1479–1514, 1998.

[65] C. Chatzichristodoulou, P. V. Hendriksen, and A. Hagen. Defect Chemistry and Thermomechanical Properties of $Ce_{0.8}Pr_xTb_{0.2-x}O_{2-d}$. *Journal of The Electrochemical Society*, 157:B299–B307, 2010.

[66] F. Wang and X. Liu. Recent Advances in the Chemistry of Lanthanide-Doped Upconversion Nanocrystals. *Chemical Society Reviews*, 38:976–989, 2009.

[67] A. Lin, X. Liu, P. R. Watekar, H. Guo, B. Peng, W. Wei, M. Lu, W. T. Han, and J. Toulouse. Intense Green Upconversion Emission in Tb^{3+}/Yb^{3+} Co-Dopedoped Alumino-Germano-Silicate Optical Fibers. *Applied Optics*, 49:1671–1675, 2010.

[68] P. N Favennec, H. L'Haridon, M. Salvi, D. Moutonnet, and Y. Le Guillou. Luminescence of erbium implanted in various semiconductors: IV, III-V and II-IV materials. *Electronic Letters*, 25:718–719, 1989.

[69] Z. Wang, Z. Quan, and J. Lin. Remarkable Changes in the Optical Properties of CeO_2 Nanocrystals Induced by Lanthanide Ions Doping. *Inorganic Chemistry*, 46:5237–5242, 2007.

[70] X. Liu, S. Chen, and X. Wang. Synthesis and photoluminescence of CeO_2:Eu^{3+} phosphor powders. *Journal of Luminescence*, 127:650–654, 2007.

[71] A. Kumar, S. Babu, A. S. Karakoti, A. Schulte, and S. Seal. Luminescence Properties of Europium-Doped Cerium Oxide Nanoparticles: Role of Vacancy and Oxidation States. *American Chemical Society*, 12:10998–11007, 2009.

[72] Y. Dimitriev, Y. Ivanova, and R. Iordanova. History of Sol-Gel Science and Technology (Review). *Journal of the University of Chemical Technology and Metalurgy*, 43:181–192, 2008.

[73] S. Sakka. Sol-Gel Technology as Reflected in Journal of Sol-Gel Science and Technology. *Journal of Sol-Gel Science and Technology*, 26:29–33, 2003.

[74] B. L. Cushing, V. L. Kolesnichenko, and C. J. O'Connor. Recent Advances in the Liquid-Phase Syntheses of Inorganic Nanoparticles. *Chemical Reviews*, 104:3893–3946, 2004.

[75] J. Silva, A. Reyes, H. Esparza, H. Camacho, and L. Fuentes. $BiFeO_3$: A Review on Synthesis, Doping and Crystal Structure. *Integrated Ferroelectrics*, 126(1):47–59, 2011.

[76] B. D. Cullity and S. R. Stock. *Elements of X-Ray Diffraction*. pages 167–171. Prentice-Hall Inc., 3rd edition edition, 2001.

[77] J. A. Wollam Co. Introduction to ellipsometry. Internet: http://www.jawoollam.com/tutorial1.html, 05 2013.

[78] L. J. Van der Pauw. *A Method of Measuring the Resistivity and Hall Coeffisient on Lamellae of Arbitrary Shape*. In *Phillips Technical Review*, volume 20, pages 220–224. 1958.

[79] A. A. Dakhel. Electrical and transport properties of europium-indium oxide films prepared on Si (1 0 0) substrates. *Physica B*, 353:255–262, 2004.

[80] Menzel-Gläser Microscope Sliders. Internet: http://www.menzel.de/Produkte.655.0.html?id=687&L=1, 06 2013. URL http://www.menzel.de/Produkte.655.0.html?id=687&L=1.

A Preparation of ITO:Tb solutions

A.1 Stoichiometry of ITO:Tb solutions

Six solutions in total of indium tin oxide (ITO) doped with terbium were prepared for modified Pechini synthesis of nanocrystalline powder and deposition of thin films by spin coating. The weighed amounts, percentage in the solution and number of moles for the different solutions are given in Table A.1. The molar masses, purities and concentration of the indium(III) nitrate precursor solution are given in Table A.2.

Table A.1: *The weighed amounts, percentage in the solution and number of moles for the prepared ITO solutions.*

ITO:0cat%Tb					ITO: 0.5cat% Tb				
g	mol	L	% measured	% desired	g	mol	L	% measured	% desired
210.8	0.000		0.0 %	90.0 %	153.7	0.0896		89.54%	89.6 %
2.367	0.010		100.0 %	10.0 %	2.356	0.010		9.95%	9.95%
			0.0 %	0.0 %	0.221	0.001		0.51%	0.5 %
9.345	0.151				9.321	0.150			
8.875	0.150				8.864	0.150			
		0.25					0.125		
	0.010					0.1000			
	0.040					0.800			
ITO: 1cat% Tb					ITO: 2cat% Tb				
g	mol	L	% meaured	% desired	g	mol	L	% measured	% desired
76.93	0.033		88.28%	89.1 %	76.18	0.033		87.32%	88.2 %
0.938	0.004		10.64%	9.9 %	0.929	0.004		10.53%	9.8 %
0.175	0.0004		1.08%	1.0 %	0.348	0.0008		2.15%	2.0 %
3.752	0.060				3.739	0.060			
3.545	0.060				3.544	0.060			
		0.10					0.10		
	0.0372					0.0372			
	0.372					0.372			
ITO: 5cat% Tb					ITO: 10cat% Tb				
g	mol	L	% measured	% desired	g	mol	L	% measured	% desired
146.7	0.0855		85.49%	85.5 %	139.0	0.0810		80.99%	81.0 %
2.250	0.010		9.50%	9.5 %	2.131	0.009		9.00%	9.0 %
2.178	0.005		5.01%	5.0 %	4.357	0.010		10.01%	10.0 %
9.314	0.150				9.315	0.150			
8.866	0.150				8.863	0.150			
		0.125					0.125		
	0.1000					0.1000			
	0.800					0.800			

Table A.2: *The molar masses, purities and concentration of the indium(III) nitrate precursor solution.*

Indium nitrate hydrate		Tin acetate hydrate		Terbium nitrate pentahydrate	
Molar mass (anhydrous) [g/mol]	Concentration solution [mol/g sol.]	Molar mass [g/mol]	Purity [%]	Molar mass [g/mol]	Purity [%]
300.8	4.27E-04	236.8		435.02	>99.99

Ethylene glycol		Acetic acid	
Molar mass [g/mol]	Purity [%]	Molar mass [g/mol]	Purity [%]
62.07	100%	59.044	99.80%

A.2 Standardisation of In(III)nitrate precursor solution

Indium(III) nitrate ($In(NO_3)_3 \cdot xH_2O$ contains variable amounts of crystal water. To be able to add the right amount of indium cations to the ITO solution, one can prepare an aqueous indium(III) nitrate solution with an approximate concentration and standardise this solution by evaporating the water in the solution. During the preparation of the indium(III)nitrate solution, we assumed that the solid contained about eight crystal water groups. Three clean calcination pots were dried at 80°C. The empty pots were weighed before approximately 30 g of solution was added to each pot and weighed accurately. The weight of the solution, calculated as the difference between these two, was named m_{sol}. The pots were then heated up to 600°C with both heating rate and cooling rate of 200°C/h, which gave a chemical reaction that resulted in indium oxide (In_2O_3) powder, given by Equation 13.

$$2In(NO_3)_3(aq) \underset{\Rightarrow}{\Delta} In_2O_3(s) + 3NO_2(g) + xH_2O(g) \tag{13}$$

The pots with dry indium oxide were weighed after the heating, and the weight of the solid powder was named m_{dry}. The concentration of the aqueous indium(III)nitrate solution could then be calculated by the formula given in Equation 14.

$$c_{In(NO_3)_3} = \frac{2m_{dry}}{M_{In_2O_3} \cdot m_{sol}} \tag{14}$$

B An introduction to ellipsometry

This appendix is a summary of "Introduction to ellipsometry" by Wollam Co. [77]. The technique of ellipsometry was developed in the 1960s to measure nanoscale layers for microelectronics and is used today for basic research in physical sciences, semiconductor and data storage solutions, flat panel displays, communication, biosensors and optical coating industries, all in which thin films play a central role. When light reflects or transmits from a material structure, a change in polarization of the light occurs. Ellipsometry measures this change and transfers the result into optical property constants and values for the thickness of the material. The polarization change is composed of two parameters, an amplitude ratio, Ψ, and a phase difference, Δ. Ellipsometry can also be used to characterize composition, crystallinity, roughness, doping concentration and other material properties associated with a change in optical response.

Light and materials Light can be described as an electromagnetic wave composed of an electric field and a magnetic field, orthogonal to each other and to the propagation direction of the light. The electric field of a wave can be described by its x- and y-component, and when light is composed of many wave which all have completely random orientations and phases, the light is considered unpolarized. In ellipsometry, however, elliptical polarized light is used, in which the light consists of two orthogonal components with arbitrary amplitude and phase. This is not the same as linearly polarized light, where the components are both orthogonal and in phase, or circularly polarized light, where the components are orthogonal and 90° out-of-phase and equal in amplitude. All cases are illustrated in Figure B.1a, B.1b and B.1c.

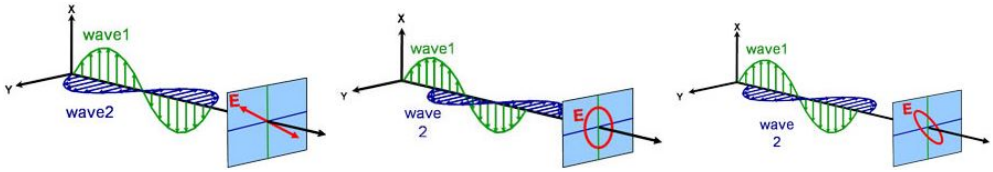

(a) *Linear* **(b)** *Circular* **(c)** *Elliptical*

Figure B.1: *Orthogonal waves combined to demonstrate polarization: (a) linear; (b) circular; and (c) elliptical.*

B.0.1 Interaction between light and materials

The complex refractive index:
The optical properties which determine how light interacts with a material, can be described by the complex refractive index, $\tilde{n}$, consisting of the real refractive index, n, and the extinction coefficient, k, as described in Equation 15.

$$\tilde{n} = n + ik \tag{15}$$

The refractive index, n, describes the speed of light as it travels in a material compared to the speed of light in vacuum, c, shown in Equation 16.

$$\nu = \frac{c}{n} \tag{16}$$

When light travels in a material, the speed decreases and the wavelength shortens since the frequency remains constant. This is related to the absorption coefficient, α, according to Equation 17.

$$\alpha = \frac{4\pi k}{\lambda} \tag{17}$$

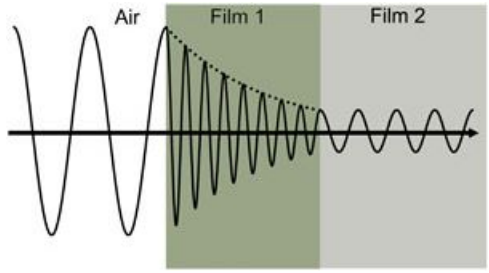

Figure B.2: *Wave travels from air into absorbing Film 1 and then transparent Film 2. The phase velocity and wavelength change in each material depending on index of refraction (Film 1: n=4, Film 2: n=2).*

At the same time, the light loses energy according to Beer's law, shown in Equation 18. The extinction coefficient, k, therefore describes how quickly the light vanishes in a material.

$$I(z) = I(0)e^{-i\alpha z} \tag{18}$$

Figure B.2 illustrates the change of properties as the light travels through layers of different refractive indices.

Refraction and reflection:
As the light hits the interface of the material, a portion of the light will be reflected, while the rest will be absorbed and refracted. The angle of the incident ray and the reflected wave will be equal, while the angle of the refracted ray is given by Snell's law, given in Equation 19. An illustration of the law is shown in Figure B.3.

$$n_0 sin(\phi_1) = n_1 sin(\phi_0) \tag{19}$$

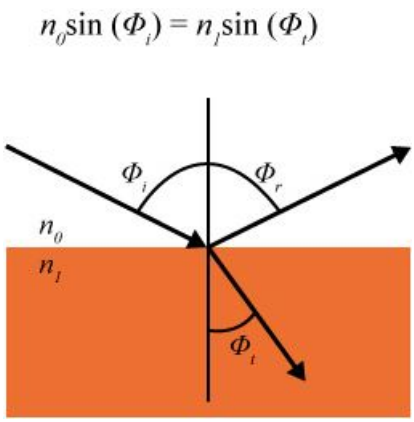

Figure B.3: *Light reflects and refracts according to Snell's law.*

Thin films and multilayer structures involve multiple interfaces, where reflection and transmission coefficients occur at each interface between the layers, described by Fresnel. The film phase thickness of each layer determines the overall reflected and transmitted beam, and is defined by Equation 20.

$$\beta = 2\pi \frac{t_1}{\lambda} n_1 cos(\phi_1) \tag{20}$$

Reflection of multiple light waves results in diffraction, illustrated in Figure B.4.

B.0.2 Ellipsometry measurements

As already described, the two components of the polarized light change phase and amplitude when interacting with a material. This change in po-

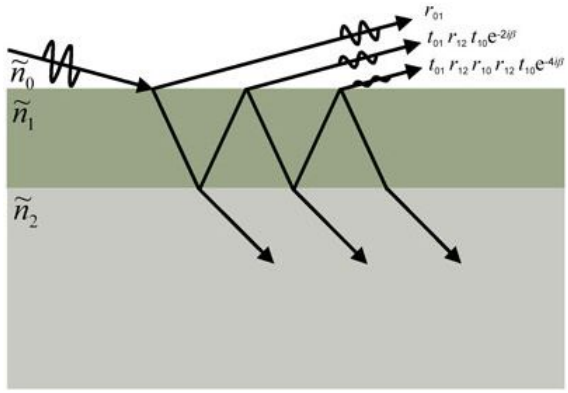

Figure B.4: *Light reflects and refracts at each interface, which leads to multiple beams in a thin film. Interference between beams depends on relative phase and amplitude of the electric fields. Fresnel refection and transmission coefficients can be used to calculate the response from each contributing beam.*

larization, measured in ellipsometry, is given in Equation 21. An illustration of an ellipsometry measurement is shown in Figure B.5.

$$\rho = tan(\Psi)e^{i\Delta} \tag{21}$$

The primary tools for collecting ellipsometry data include the following: light source, polarization generator, sample, polarization analyzer, and detector. The polarization generator and analyzer are constructed of optical components that manipulate the polarization: polarizers, compensators, and phase modulators. A light source produces white light which is then polarized. The polarizer allows light of a preferred electric field orientation to pass. The linearly polarized light reflects from the sample surface, becomes elliptically polarized, and travels through a continuously rotating

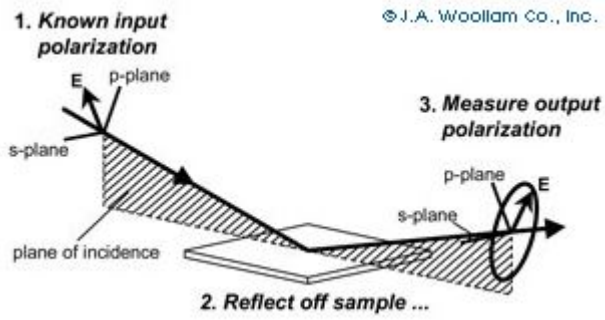

Figure B.5: *Typical ellipsometry configuration, where linearly polarized light is reflected from the sample surface and the polarization change is measured to determine the sample response.*

polarizer (referred to as the analyzer). The amount of light allowed to pass will depend on the polarizer orientation relative to the electric field "ellipse" coming from the sample. The detector converts light to electronic signal to determine the reflected polarization. This information is compared to the known input polarization to determine the polarization change caused by the sample reflection, given by the amplitude change, Ψ, and the phase change, Δ.

B.0.3 Data analysis

When analyzing the ellipsometry measurements, a model is constructed and a by regression method, the experimental data is fitted to this model by varying the material properties, such as thickness, roughness and uniformity.

The thickness is determined from the interference between the reflection light from the top surface and the bottom surface of the film. The thicker the film, the more difficult it is to distinguish the constructive interference

lines. The film also needs to be transmittant enough so that light can travel through the film and back again.

C Rietveld refinement of crystal structure

Table C.1 shows some of the parameters used in the Rietveld refinement of the nanocrystalline ITO:Tb thin films, while Table C.2 shows the parameters for the associated powders. Figures B.1-B.23 show the Rietveld refinement fitting for all the samples. The refinement was used to extract information about the lattice parameter of the cubic crystal structure and the crystallite size using the integral breadth approach (numbers are emphasized by the color green).

Table C.1: *Rietveld refinement parameters for the ITO:Tb thin films. The lattice parameter and the crystallite size calculated by the volume averaged column height by integral breadth (Lvol-IB) are emphasized by the color green.*

Sample	Tb conc [%]	Cat.conc [M]	# layers	Lattice parameter	Error	Lvol-IB [nm]	Error	LVol-FWHM [nm]	Error	Rwp
ITO_10	0	0.2	10	10.1386	0.0065	6.89	0.931	9.63	0.774	1.893
05Tb_3	0.5	0.4	3	10.1266	0.0013	9.46	0.274	12.96	0.425	1.599
05Tb_7			7	10.1348	0.0009	9.87	0.227	12.83	0.319	1.904
05Tb_10			10	10.1347	0.0007	10.42	0.196	12.87	0.246	1.938
05Tb_10_ox			10	10.1276	0.0015	9.67	0.350	12.82	0.508	1.555
1Tb_3	1	0.2	3	10.1211	0.0011	10.26	0.303	13.75	0.414	1.312
1Tb_7			7	10.1276	0.0007	9.90	0.188	12.09	0.228	1.448
1Tb_10			10	10.1292	0.0009	9.75	0.143	11.95	0.168	1.519
1Tb_10_ox			10	10.1316	0.0012	10.15	0.343	12.87	0.452	1.477
2Tb_10	2	0.2	10	10.1344	0.0009	9.74	0.228	12.05	0.287	1.999
5Tb_3	5	0.4	3	10.1316	0.0012	10.17	0.345	12.86	0.453	1.477
5Tb_7			7	10.1370	0.0012	9.51	0.295	12.16	0.396	2.548
5Tb_10			10	10.1416	0.0009	9.96	0.225	12.60	0.296	1.547
5Tb_10_ox			10	10.1434	0.0008	9.74	0.206	12.27	0.269	1.665
10Tb_3	10	0.4	3	10.1320	0.0013	10.49	0.389	13.48	0.530	1.552
10Tb_7			7	10.1424	0.0011	9.86	0.281	12.51	0.373	2.038
10Tb_10			10	10.1506	0.0010	10.20	0.236	12.99	0.318	2.221
10Tb_10_ox			10	10.1510	0.0010	10.16	0.252	12.61	0.320	1.995
				Average crystallite size		9.79		12.52		

Table C.2: *Rietveld refinement parameters for the ITO:Tb powders. The lattice parameter and the crystallite size calculated by the volume averaged column height by integral breadth (Lvol-IB) are emphasized by the color green.*

0Tb	0	0.2	10.1310	0.0007	11.01	0.172	14.03	0.238	3.372
05Tb	0.5	0.4	10.1198	0.0006	11.75	0.153	15.49	0.231	3.248
1Tb	1	0.2	10.1303	0.0006	10.36	0.139	12.99	0.183	2.792
2Tb	2	0.2	10.1444	0.0008	12.17	0.251	15.46	0.343	4.373
5Tb	5	0.4	10.1290	0.0005	14.63	0.203	19.96	0.325	2.977
10Tb	10	0.4	10.1320	0.0006	13.67	0.207	18.47	0.322	2.759

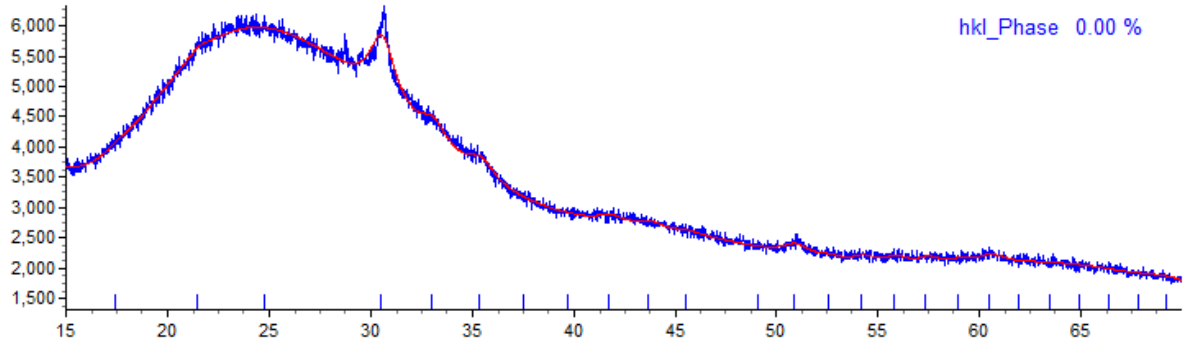

Figure B.1: ITO:0cat%Tb:10 layer thin film

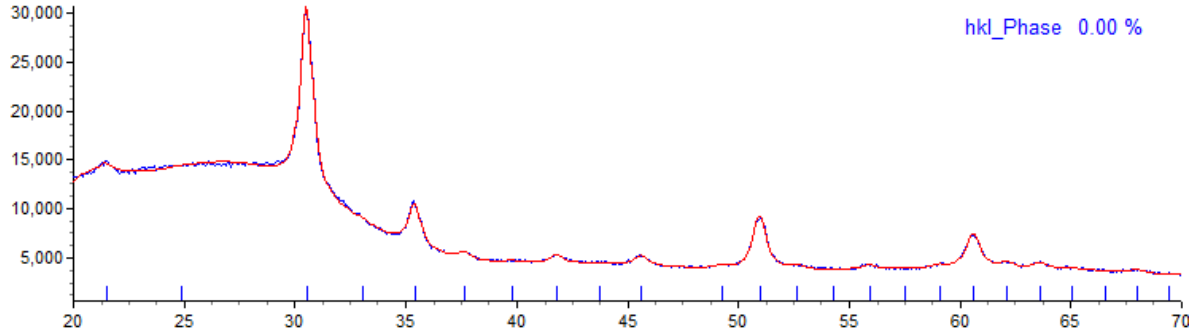

Figure B.2: ITO:0.5cat%Tb:3 layer thin film

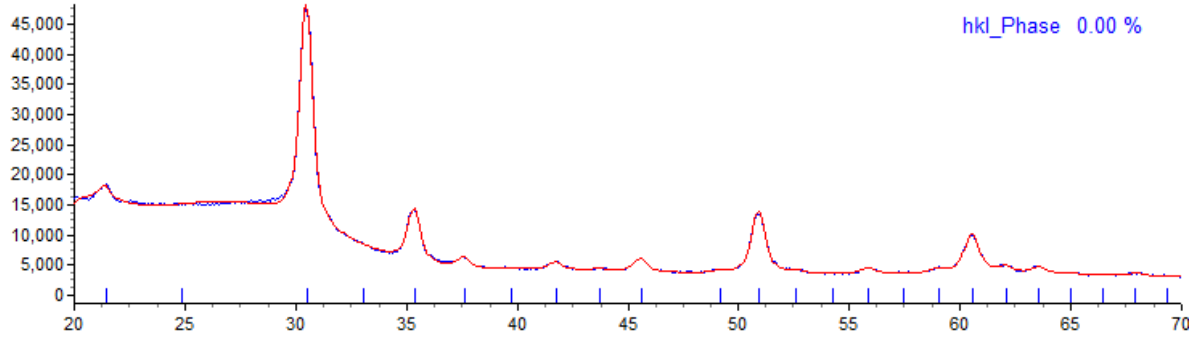

Figure B.3: ITO:0.5cat%Tb:7 layer thin film

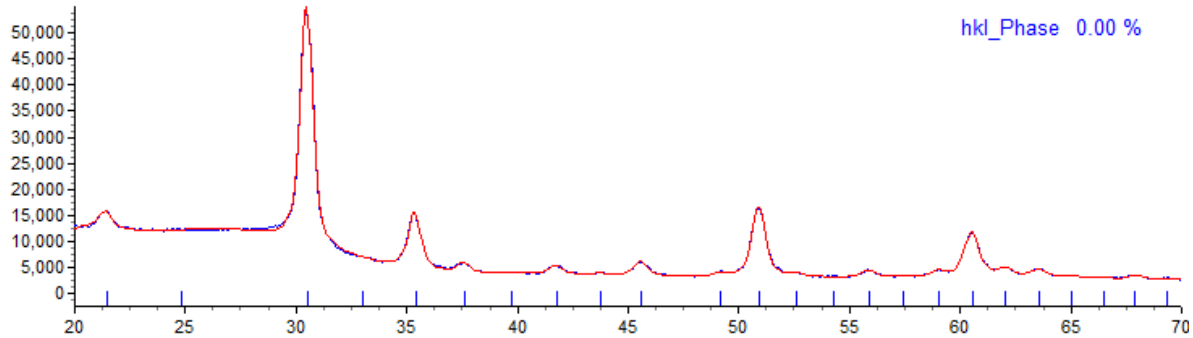

Figure: B.4: ITO:0.5cat%Tb:10 layer thin film

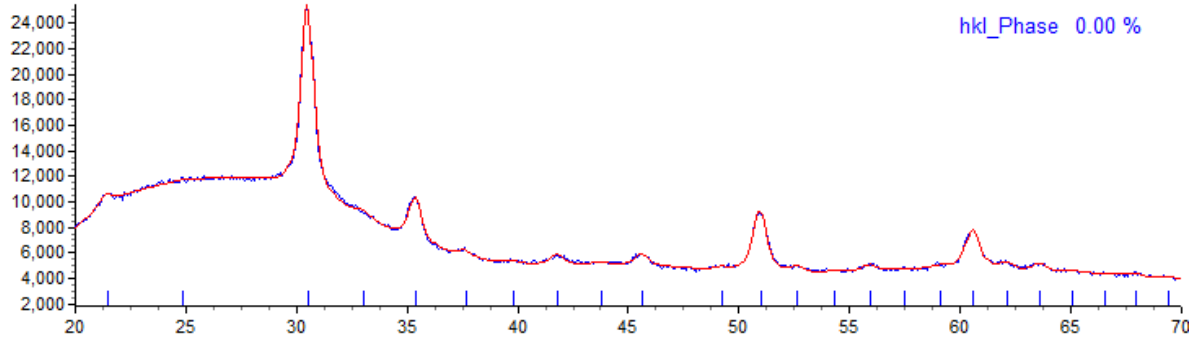

Figure B.5: ITO:0.5cat%Tb:10 layer thin film, heat-treated in air

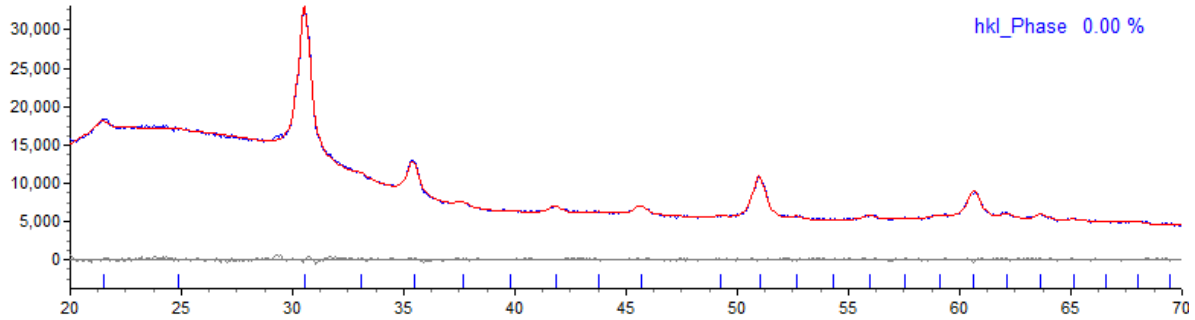

Figure B.6: ITO:1cat%Tb:3 layer thin film

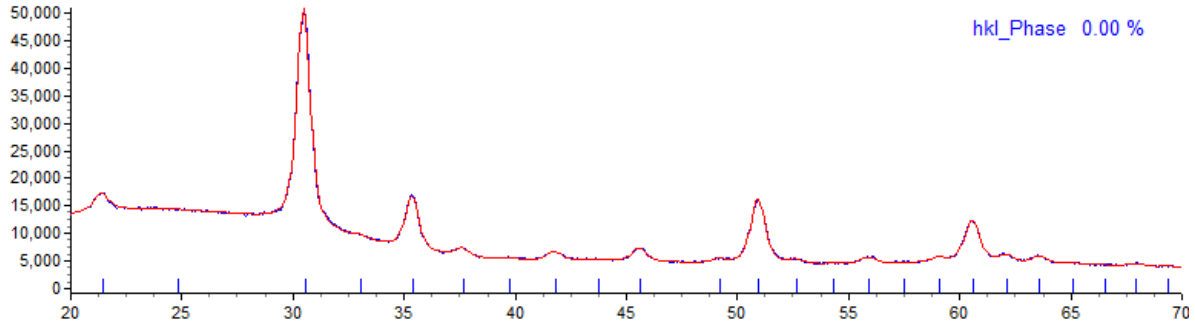

Figure B.7: ITO:1cat%Tb:7 layer thin film

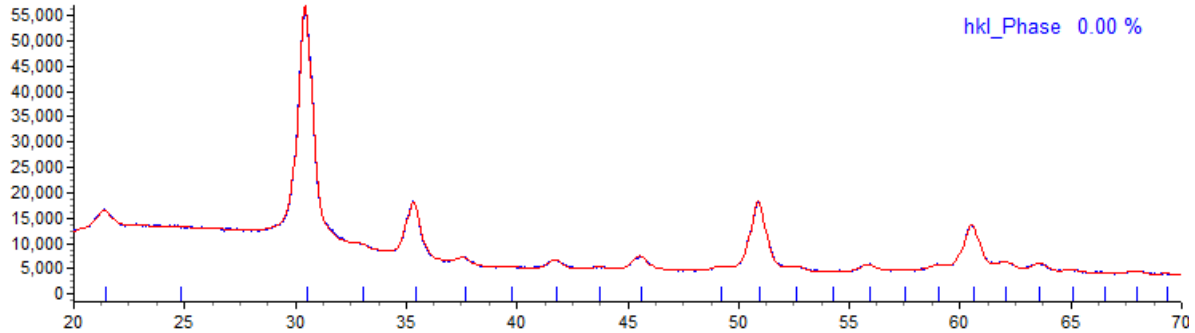

Figure B.8: ITO:1cat%Tb:10 layer thin film

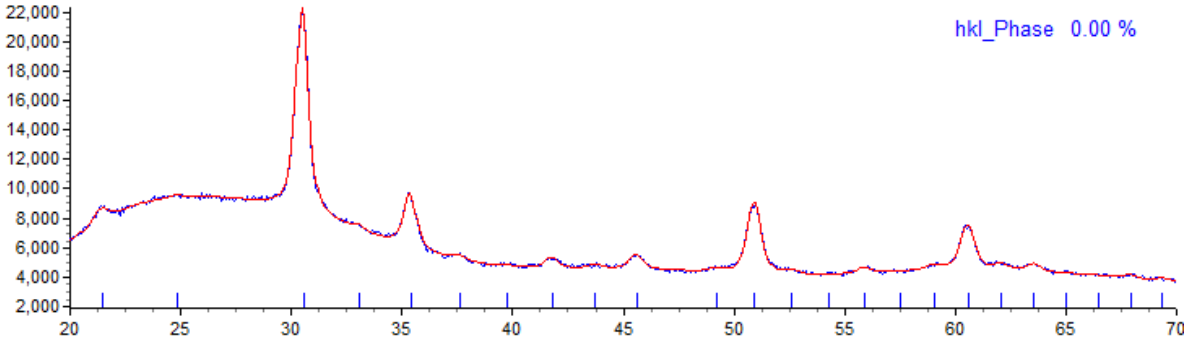

Figure B.9: ITO:1cat%Tb:10 layer thin film, heat-treated in air

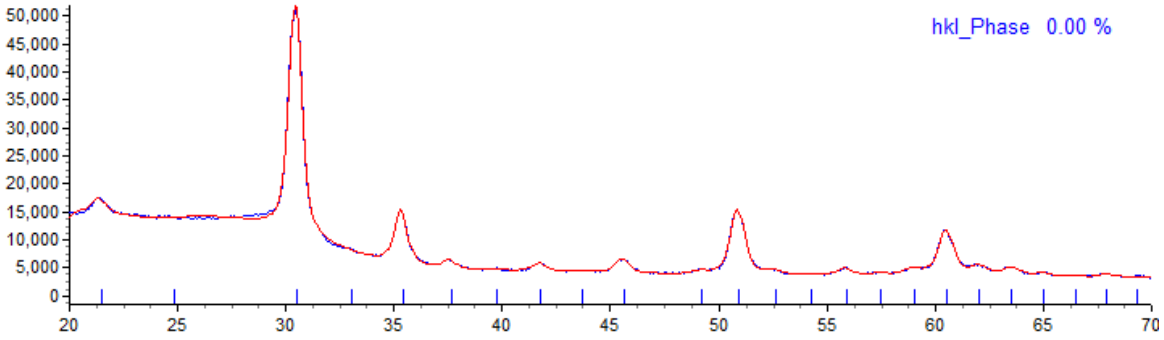

Figure B.10: ITO:2cat%Tb:10 layer thin film

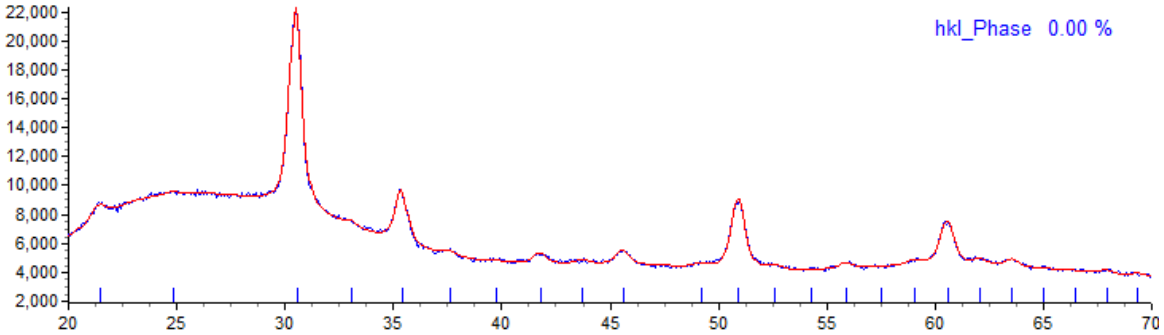

Figure B.11: ITO:5cat%Tb:3 layer thin film

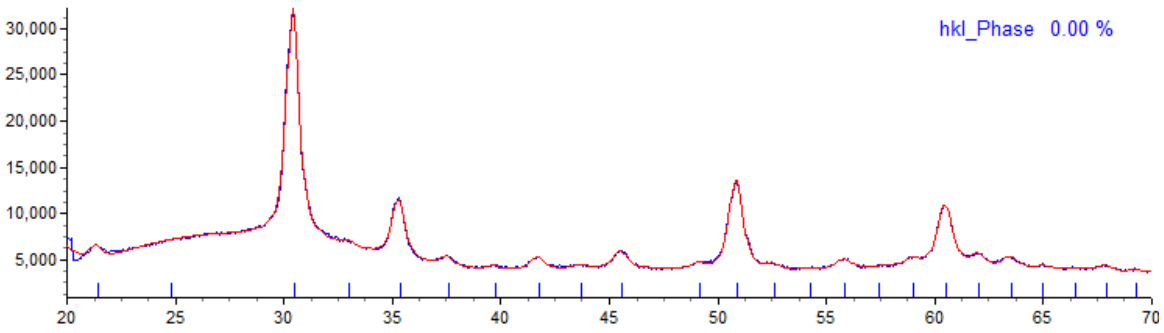

Figure B.12: ITO:5cat%Tb:7 layer thin film

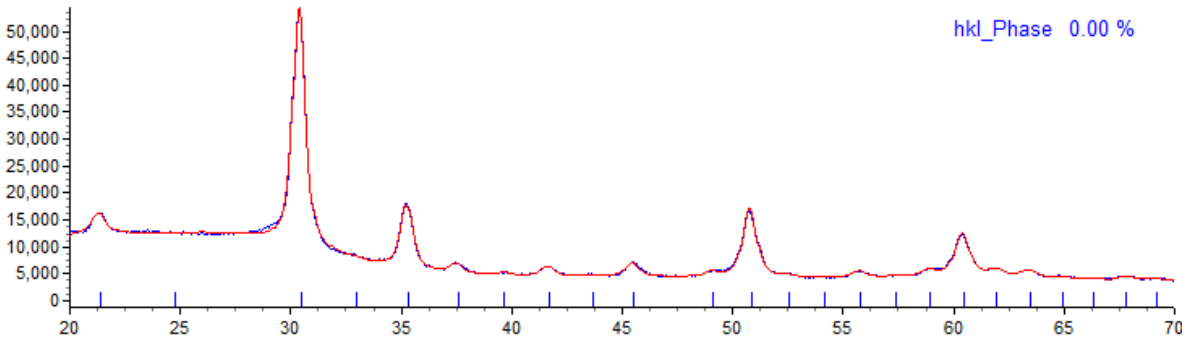

Figure B.13: ITO:5cat%Tb:10 layer thin film

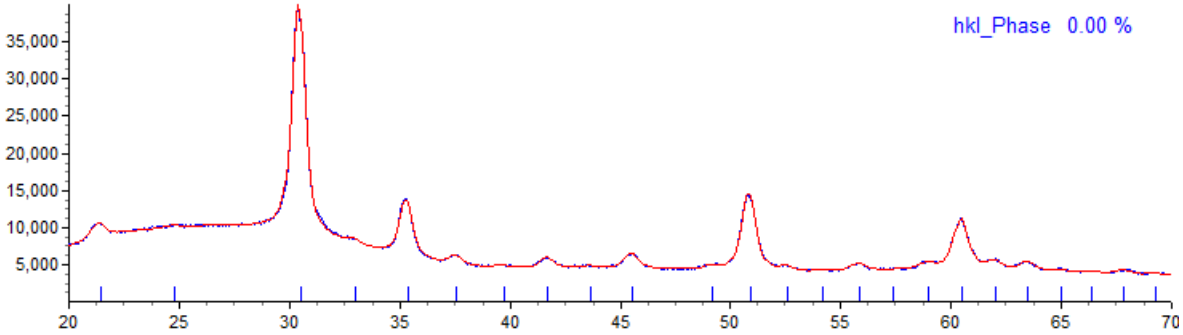

Figure B.14: ITO:5cat%Tb:10 layer thin film, heat-treated in air

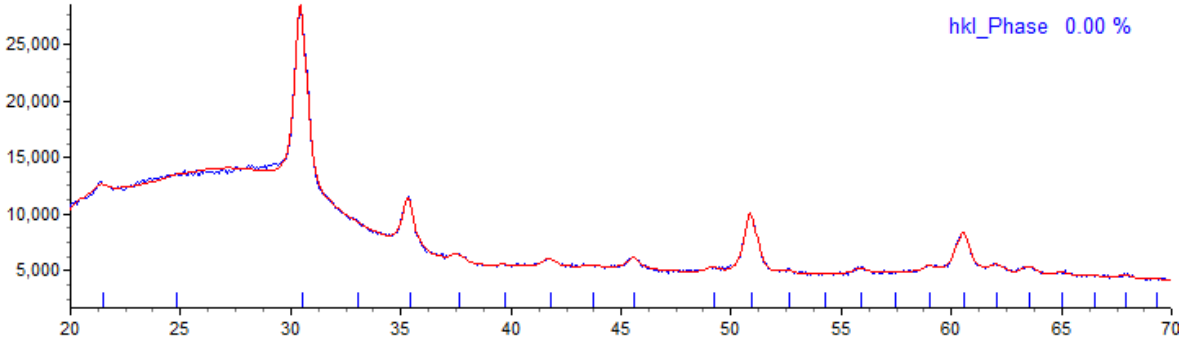

Figure B.15: ITO:10cat%Tb:3 layer thin film

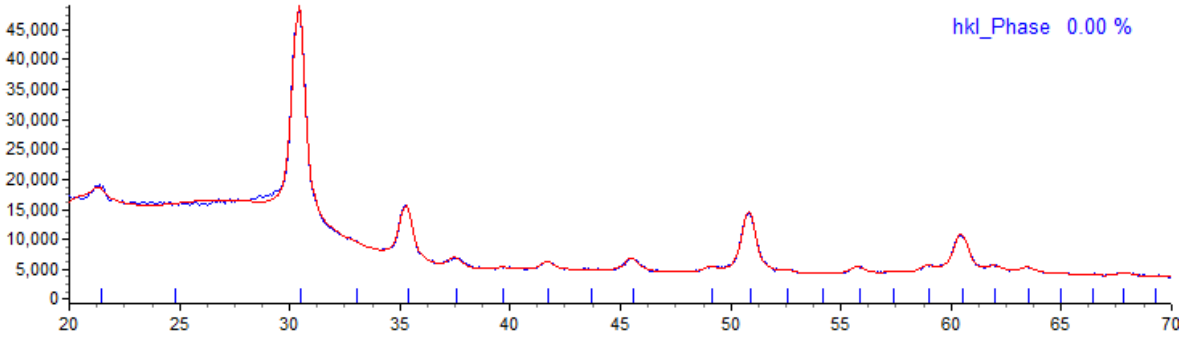

Figure B.16: ITO:10cat%Tb:7 layer thin film

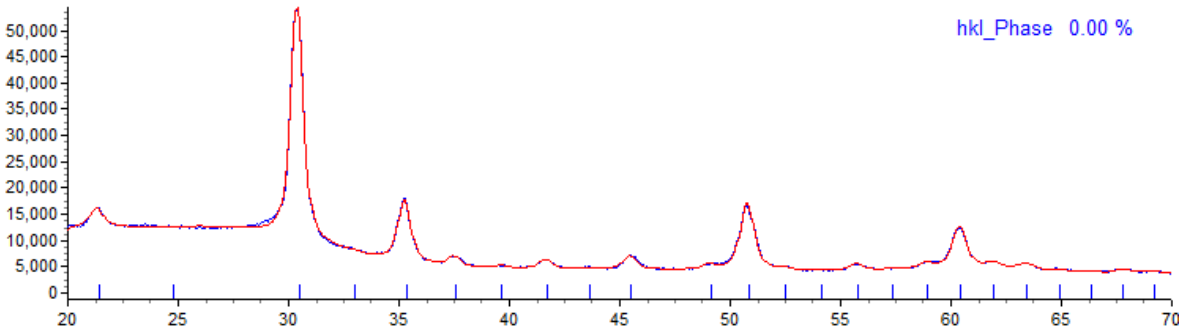

Figure B.17: ITO:10cat%Tb:10 layer thin film

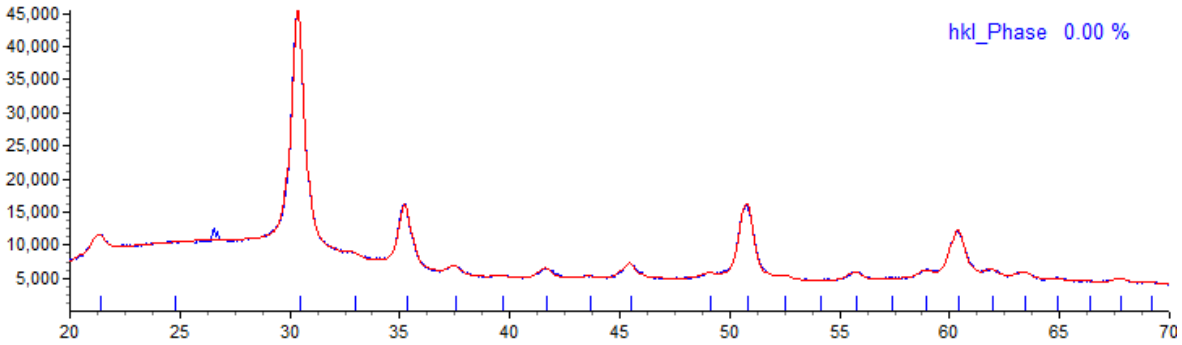

Figure B.18: ITO:10cat%Tb:10 layer thin film, heat-treated in air

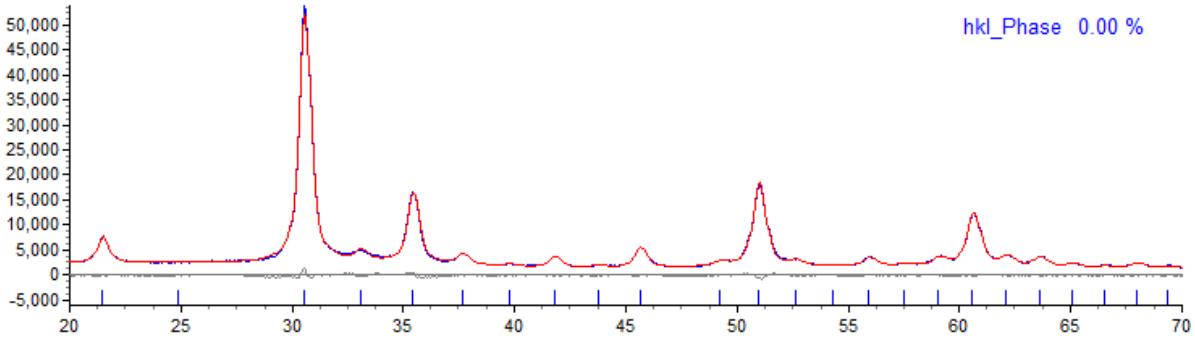

Figure B.19: ITO:0cat%Tb powder

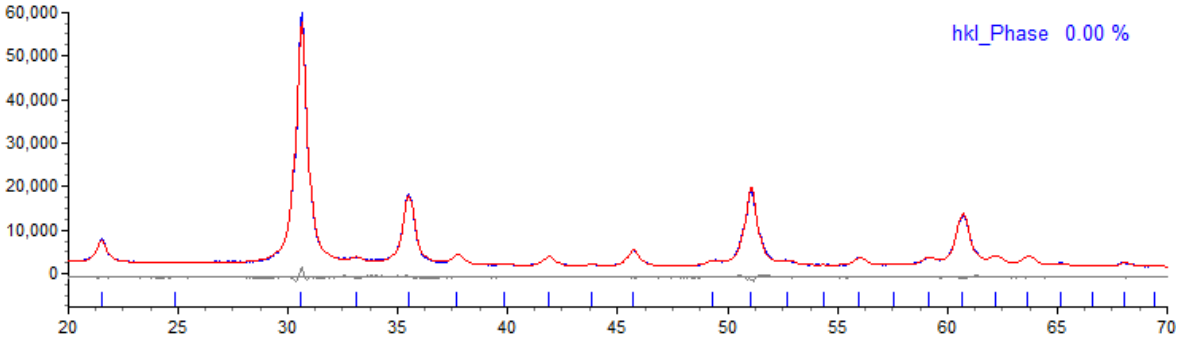

Figure B.20: ITO:0.5cat%Tb powder

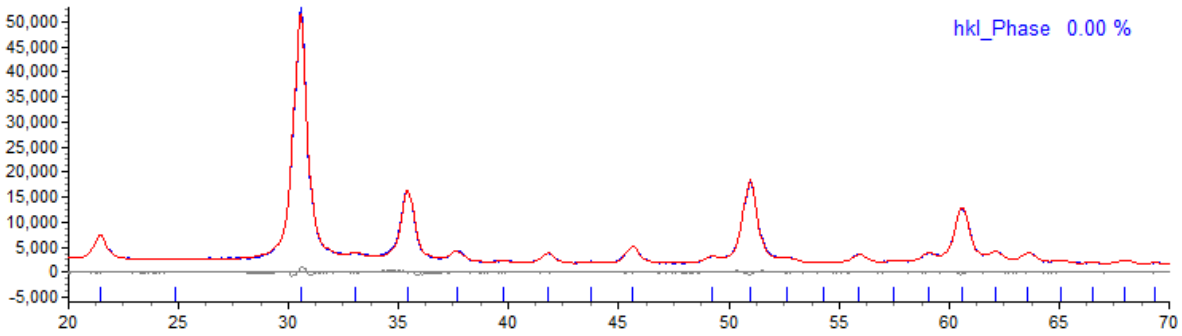

Figure B.21: ITO:1cat%Tb powder

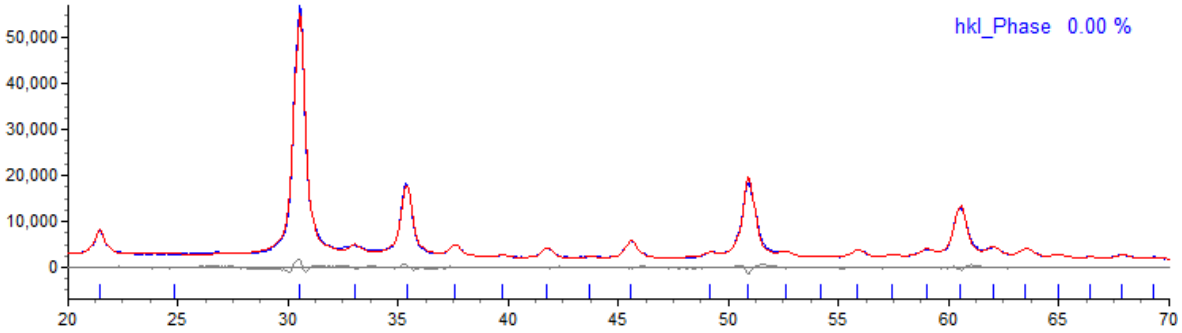

Figure B.21: ITO:2cat%Tb powder

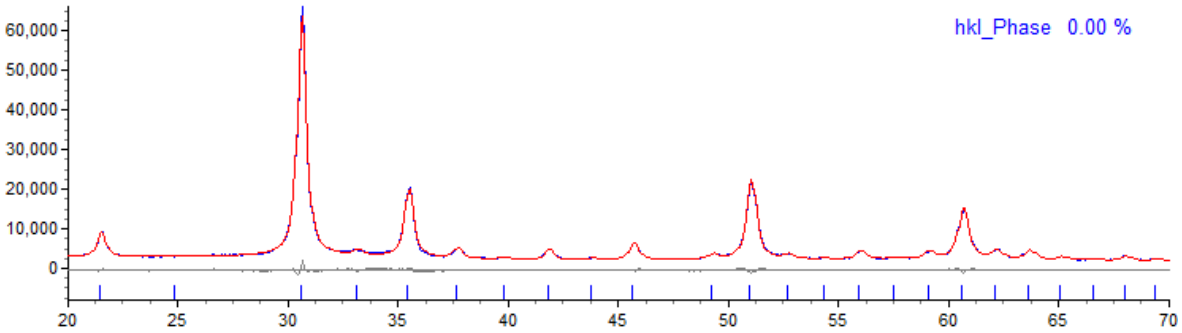

Figure B.22: ITO:5cat%Tb powder

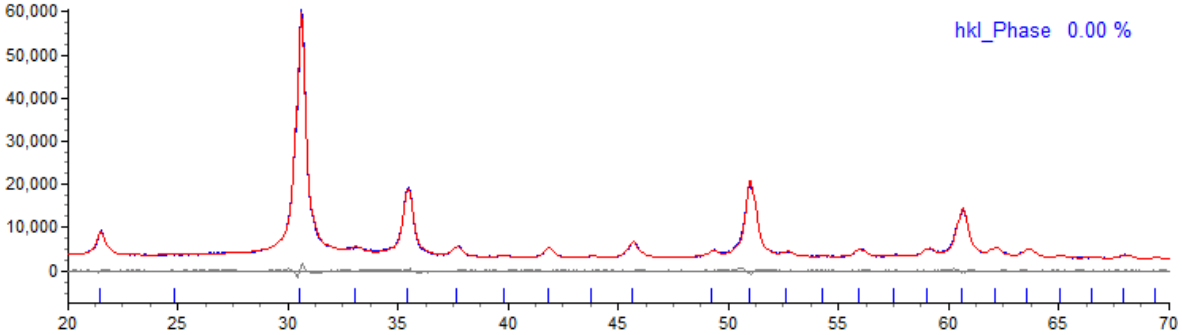

Figure B.23: ITO:10cat%Tb powder

D Average grain size of the surface particles

The grain size on the surface was measured for two thin films. Utilising the scanning electron microscopy images, a ruler was used to measure the length of three adjacent particles at random positions on the surface. Dense areas where particles were positioned in a line were preferred so that porosity could be neglected and the whole diameter of the particles was measured. Table D.1 shows the measurements and the calculations.

Table D.1: *Calculation of the average grain size on the surface of two thin films.*

Sample	Measurement	Length of 3 particles (cm)
10% Tb	1	2.05
	2	2.20
Scale of picture	3	1.80
3.0 cm = 100 nm	4	1.90
	5	2.05
	6	2.40
	7	2.00
	8	1.80
	9	1.80
	10	1.90
Average of measurements		**1.99**
Average particle size	$= \frac{L}{\#\,part.} \times scale$ $= \frac{1.99cm \times 100nm}{3 \times 3.0cm}$	**22**
Standard deviation		**1**

Sample	Measurement	Length of 3 particles (cm)
0.5% Tb	1	2.10
	2	2.20
Scale of picture	3	2.40
3.1 cm = 100 nm	4	2.20
	5	1.90
	6	2.10
	7	2.00
	8	1.90
	9	2.60
	10	2.00
Average of measurements		**2.14**
Average particle size	$= \frac{L}{\#\,part.} \times scale$ $= \frac{2.14cm \times 100nm}{3 \times 3.1cm}$	**23**
Standard deviation		**1**

E Change in charge carrier concentration

Table E.1 shows the calculated values for the reduction in charge carriers, amount of terbium ions in the samples and the fraction of oxidized terbium ions.

Table E.1: *Calculated change in number of charge carriers, number of terbium ions in the sample and fraction of oxidized terbium ions.*

Sample	cat% Tb	Temp. Pre-heat [C]	Cond. Pre-heat [S/cm]	Temp. Heat-treated [C]	Cond. Heat-treated [S/cm]
ITO	0	20	0.0149	21	0.00461
2% Tb ITO	2	23	0.0081	23	0.00218
5% Tb ITO	5	20	0.0049	-	0.00036
10% Tb ITO	10	20	0.0020	21	0.00002

Reduction from pre-heat to heat-treated	Reduction charge carriers	Reduction due to Tb	Initial Tb atoms per unit cell	Lattice parame. pre-heat [Å]	Volume unit cell [cm]	Initial Tb per volume [/cm]	Fraction oxidized Tb
69%	4.30E+15	0.00E+00	0	10.1386	1.042E-21	0.00E+00	0
73%	2.45E+15	7.55E+14	64	10.1344	1.041E-21	6.15E+22	1.23E-08
93%	1.90E+15	5.85E+14	160	10.1416	1.043E-21	1.53E+23	3.82E-09
99%	8.09E+14	2.50E+14	320	10.1506	1.046E-21	3.06E+23	8.16E-10

The difference in conductivity and the reduction in charge carriers was calculated by the formula in Equation 22 and 23.

$$change = \frac{conductivity\,after - conductivity\,pre}{conductivity\,pre} \tag{22}$$

$$Reduction\,charge\,carriers = \frac{reduction}{e\mu_e} \tag{23}$$

Electrical mobility (μ_e): 15 cm^2/Vs, elementary charge (e): $1.60 \cdot 10^{-19}C$, Avogadro's number (N_A): $6.022 \cdot 10^{-23}C$, cations per unit cell: 32.